

Pre-trained Encoder Inference: Revealing Upstream Encoders In Downstream Machine Learning Services

Shaopeng Fu*, Xuexue Sun[†], Ke Qing[‡], Tianhang Zheng[§] and Di Wang*

*King Abdullah University of Science and Technology, {shaopeng.fu, di.wang}@kaust.edu.sa

[†]HitoX, snows.yanzhi@gmail.com

[‡]University of Science and Technology of China, qingkeld@mail.ustc.edu.cn

[§]Zhejiang University, zthzheng@gmail.com

Abstract—Though pre-trained encoders can be easily accessed online to build downstream machine learning (ML) services quickly, various attacks have been designed to compromise the security and privacy of these encoders. While most attacks target encoders on the upstream side, it remains unknown how an encoder could be threatened when deployed in a downstream ML service. This paper unveils a new vulnerability: the *Pre-trained Encoder Inference (PEI)* attack, which posts privacy threats toward encoders hidden behind downstream ML services. By only providing API accesses to a targeted downstream service and a set of candidate encoders, the PEI attack can infer which encoder is secretly used by the targeted service based on candidate ones. We evaluate the attack performance of PEI against real-world encoders on three downstream tasks: image classification, text classification, and text-to-image generation. Experiments show that the PEI attack succeeds in revealing the hidden encoder in most cases and seldom makes mistakes even when the hidden encoder is not in the candidate set. We also conducted a case study on one of the most recent vision-language models, LLaVA, to illustrate that the PEI attack is useful in assisting other ML attacks such as adversarial attacks. The code is available at <https://github.com/fshp971/encoder-inference>.

I. INTRODUCTION

Recent advances of self-supervised learning (SSL) [1, 2, 3, 4, 5, 6] and the availability of large amounts of public unlabeled data have enabled the pre-training of powerful representation encoders. These pre-trained encoders are usually first built by upstream suppliers who control sufficient computational resources and then delivered through online model repositories (e.g., Hugging Face¹) or *Encoder-as-a-Service (EaaS)* to downstream suppliers to help them quickly build their own machine learning (ML) services. Specifically, one can simply use an encoder to encode downstream training data to informative embeddings and train downstream models upon them with relatively little cost. These downstream models are eventually provided as service APIs to end users.

Despite the success of this *upstream pre-training, downstream quick-building* paradigm, many attacks have also emerged to threaten the security and privacy of pre-trained encoders. Current attacks toward pre-trained encoders can be roughly divided into two categories: The first category aims to attack encoders in the SSL stage via poisoning [7, 8] or back-dooring [9, 10, 11, 12] to manipulate their behaviors, while the second one targets trained encoders and aims to extract private information of their training data [13, 14, 15] or unauthorizedly

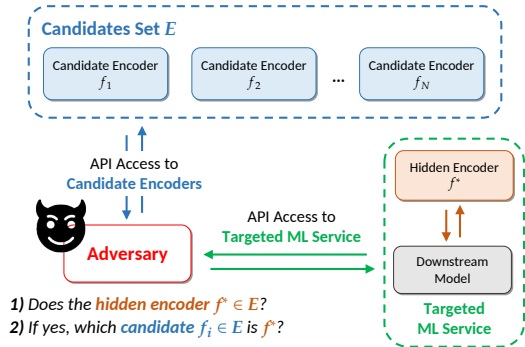


Fig. 1: An illustration of the threat model of the PEI attack. In this model, the adversary has API accesses to a set E of candidate encoders and a targeted downstream ML service built upon a hidden encoder f^* . The attack goal is to infer whether the hidden encoder f^* is in the candidate set E , and if so, further infer which candidate $f_i \in E$ is the hidden f^* .

duplicate their encoding functionalities [16, 17, 18]. To mitigate these attacks, various defenses are designed to enhance the robustness of encoders against adversaries [19, 20, 21] or perform source tracing when an attack has occurred [22, 23, 24].

While attacks and defenses toward bare pre-trained encoders on the upstream side have been vastly studied, encoders that have already been deployed in downstream services do not receive equal attention, which may be due to the common belief that they are usually much safer on the downstream side. Concretely, when a pre-trained encoder is deployed in a downstream service, the end users can only see and access the service APIs powered by the downstream model. In this way, the downstream model seems like a shield that isolates the encoder from end adversaries, leaving them unable to interact directly with it using malicious queries. Though such a “downstream protection” is supported by the *data processing inequality* to some extent, it is still not quantified how much the information of the hidden encoder is sanitized through the downstream model and APIs. Thus, it remains open whether and how a pre-trained encoder deployed in a downstream ML service could be threatened by malicious end users.

Our works. This paper shows that pre-trained encoders can indeed be threatened from the downstream side by introducing a new class of privacy attacks named *Pre-trained Encoder*

¹Hugging Face model repository is at <https://huggingface.co/models>.

Inference (PEI) attack. As illustrated in Figure 1, by providing a set E consisting of several candidate pre-trained encoders, for a targeted downstream ML service that is built upon a hidden encoder f^* (note that f^* may not in E), the PEI attack will infer whether the hidden encoder f^* comes from the candidate set E . Furthermore, if the hidden encoder is inferred to be from the candidate set, the PEI attack will reveal which candidate encoder is the targeted hidden encoder. A key feature makes our PEI attack very practical in the real world: the adversary only requires *API access* to candidate encoders and the targeted ML service to perform the PEI attack.

The design of the PEI attack is motivated by the observation that for any certain encoder and a pre-defined embedding, there may exist samples that look different from each other but enjoy embeddings similar to that pre-defined embedding only under such a certain encoder. Therefore, we propose a general framework to implement the PEI attack by first synthesizing a series of *PEI attack samples* via minimizing the difference of their embeddings and the pre-defined embedding under the certain encoder from the candidate set, and then inferring whether this certain candidate encoder is used by a targeted downstream ML service by evaluating whether these synthesized PEI attack samples can make the targeted service produce a specified behavior determined by that pre-defined embedding. Since in our threat model, the adversary only has API access to candidate encoders, the PEI attack further exploits zeroth-order optimization [25, 26, 27] to synthesize PEI attack samples for different candidate encoders. Besides, it is worth noting that while the synthesis of PEI attack samples depends on specific data modalities, our attack framework makes no other assumptions about the downstream tasks. Thus, in other words, the PEI attack is downstream task-agnostic as long as the input data modality is given, which is another advantage of our attack: once the PEI attack samples are synthesized, the adversary can use them to attack any kind of downstream ML services.

While the aforementioned general attack framework can be applied to encoders on any data modalities, in this work we focus on analyzing two families of encoders: *image encoders* and *text encoders*. We conduct experiments to evaluate the PEI attack against different image/text encoders in three downstream tasks: image classification, text classification, and text-to-image generation. Results show that the PEI attack successfully reveals correct hidden encoders from 24 out of 24 image classification services, 14 out of 24 text classification services, and 4 out of 4 text-to-image services. The PEI attack also demonstrates a strong capability in avoiding false-positive predictions: it seldom infers incorrect encoders as the hidden ones even when the correct hidden encoder is not in the candidate set. This feature is handy for adversaries as they do not need to waste time in tackling false-positive signals and thus will always have a good chance to find a victim in a short time after many unsuccessful but quick tries. In addition to the significant attack performance and practicality, the cost of black-box synthesizing PEI attack samples is also low, with an estimated price of no more than \$400 per candidate encoder.

We further argue that the PEI attack is useful in practice by conducting a case study on how the PEI attack can assist adversarial attacks against LLaVA [28, 29], a recent multimodal model. The overall attack goal is to synthesize *visually benign*

adversarial images to induce LLaVA to generate malicious textual content. Concretely, the adversary will first use the PEI attack to reveal the image encoder hidden in LLaVA. With direct access to this hidden encoder, the adversary will then synthesize adversarial images that contain only benign mosaics but enjoy embeddings very similar to images that contain pre-defined harmful texts. As a result, when feeding these synthesized mosaic images to LLaVA, the model will generate texts that are similar to the pre-defined harmful contents. Such a PEI-assisted adversarial attack can be used to stealthily spread harmful information such as false medical/health information or hate speeches, since the spreading mediums, *i.e.*, the mosaic adversarial images, do not contain visually harmful information and thus are difficult to be detected and filtered. As a result, there is indeed a practical need to develop general defenses against the PEI attack.

Finally, as a preliminary investigation, we discuss potential defenses against the PEI attack, which include methods that sanitizing or detecting PEI attack samples, or re-designing downstream models to be natively robust to the PEI attack.

Contributions. In summary, our work makes the following contributions: (1) We unveil a new vulnerability of pre-trained encoders named *Pre-trained Encoder Inference (PEI)* attack that can reveal what encoder is secretly used by a targeted downstream ML service (Section III-B). (2) We propose a general framework to implement the PEI attack in a black-box and downstream task-agnostic manner (Section IV), and instantiate it for image encoders and text encoders (Section V). (3) We empirically verify the effectiveness of the PEI attack on three families of downstream tasks, which are image/text classifications (Section VI), and text-to-image generation (Section VII). (4) We conduct a case study on LLaVA to show how the PEI attack can assist adversarial attacks against multimodal models (Section VIII). The result demonstrates the usefulness of the PEI attack and thus calls for a practical need to develop defenses against the PEI attack. (5) Finally, we discuss several potential defenses against the PEI attack (Section IX).

II. RELATED WORKS

Privacy attacks. Existing ML privacy attacks can be roughly divided into two categories, which are *data privacy attacks* and *model privacy attacks*. Concretely, data privacy attacks include membership inference attacks (MIA) [30, 31, 32, 33, 34, 35] which aim to infer whether a given sample comes from training set or not, and data reconstruction attacks (DRA) [36, 37, 38] which aim to extract exact training samples based on model outputs or gradients. Recent studies find that data privacy attacks can be enhanced through poisoning targeted models [39]. On the other hand, model privacy attacks focus on extracting private information of models such as training hyperparameters [40], architectures [41, 42, 43, 44], model parameters [45, 46], and functionalities [47, 48, 49]. Our PEI attack also falls under the category of model privacy attacks. Unlike existing approaches, the PEI attack aims to infer a specific component of the architecture of downstream ML services, *i.e.*, the used pre-trained encoder.

Privacy attacks against pre-trained encoders. For data privacy attacks, many efforts have been made to design MIA against encoders. When the pre-training strategy is known, [13]

successfully performs membership inference attacks (MIA) against targeted encoder based on membership scores calculated with the pre-training loss function and shadow training techniques. [14] extends MIA against semi-supervisedly learned encoders. [15] studies a more challenging setting where the adversary has no knowledge about pre-training algorithms and proposes to calculate the embedding similarity between global and local features as the membership score for each sample. [11] and [12] show that backdoored encoders can increase the privacy vulnerabilities of downstream models built upon them. Besides, for model privacy attacks, studies mainly focus on stealing the powerful encoding functionality of encoders. By simply querying the targeted encoder and collecting return embeddings, [16] succeeds in retraining an encoder that reproduces the functionality of the target with a reasonable query budget. [17] adopted a contrastive learning-based method to further improve the encoder stealing performance. However, all these data/model privacy attacks usually require detailed information about the downstream tasks, such as the number of classes in downstream classification tasks or prior knowledge of potential targeted training data, which may limit their practicality in the real world. As a comparison, our PEI attack can work in a downstream task-agnostic manner.

III. PRELIMINARIES

A. Pre-trained Encoders

A pre-trained encoder is a function $f : \mathcal{X} \rightarrow \mathcal{E}$ that can encode any sample point $x \in \mathcal{X}$ to an informative embedding vector $f(x)$. This powerful encoding ability can be used to facilitate building downstream ML services, (e.g., image/text classification, and text-to-image generalization). Specifically, suppose there is a downstream task-specific dataset $D = \{(x_i, y_i)\}_{i=1}^{|D|}$, where $x_i \in \mathcal{X}$ is the i -th downstream sample and $y_i \in \mathcal{Y}$ is its corresponding label. To build an ML service to handle the downstream task, the service supplier will encode each downstream sample x_i to $f(x_i)$, and train a downstream model h_θ on these encoded embeddings as follows,

$$\min_{\theta} \frac{1}{|D|} \sum_{(x_i, y_i) \in D} \ell(h_\theta(f(x_i)), y_i),$$

where $\ell : \mathcal{Y} \times \mathcal{Y} \rightarrow \mathbb{R}^+$ is a downstream task-dependent loss function and θ is the downstream model parameter. After that, the downstream ML service will be made online and provide API access to end users, in which the API is powered by the composite function $h_\theta(f(\cdot)) : \mathcal{X} \rightarrow \mathcal{Y}$. Whenever a query x comes, the service API will return $h_\theta(f(x))$ as the response.

B. Threat Model

The threat model of the PEI attack is illustrated in Figure 1, which consists of two parties: (1) a targeted downstream ML service $g : \mathcal{X} \rightarrow \mathcal{Y}$, and (2) the adversary. We next introduce them in detail.

Downstream ML service g . The service can be seen as a composite function $g(\cdot) := h_\theta(f^*(\cdot))$, where f^* is the encoder secretly used in the downstream service and h_θ is the downstream model trained following the pipeline described in Section III-A. It is notable that this targeted service g can only

be accessed through APIs: for any query sample x from end-users, the service will only return $g(x)$ as the response. Other operations are not allowed.

Adversary’s goal. The overall goal of the adversary is to reveal the encoder f^* hidden by the targeted service g . Concretely, suppose the adversary holds a set $E = \{f_1, \dots, f_N\}$ consisting of N publicly accessible pre-trained encoders that may come from online model repositories or EaaS. Then, the adversary aims to: (1) determine whether the hidden encoder f^* comes from the candidates set E , and (2) if it is determined that $f^* \in E$, infer which candidate $f_i \in E$ is the hidden f^* .

Adversary’s capabilities. We assume that the adversary has the following capabilities:

- **API access to the targeted service.** The adversary can query the targeted service g with any sample x and receive the return $g(x)$. It is notable that the adversary has no prior knowledge about the downstream model h_θ and the hidden encoder f^* and is not allowed to directly interact with the hidden f^* through g .
- **API access to candidate encoders.** For each candidate $f_i \in E$, the adversary can query it with any sample x and receive the return $f_i(x)$. However, the adversary could not access the model parameter of f_i . We argue that the size of the candidate set would not be too large, as real-world applications usually tend to use EaaS/pre-trained encoders provided by a few reputable tech companies (e.g., OpenAI, Hugging Face, Microsoft, and Google).

IV. PEI ATTACK FRAMEWORK

In this section, we present a general framework to perform the PEI attack. At a high level, our designed framework is motivated by the hypothesis that for a certain encoder and a pre-defined embedding, there may exist samples that look different but enjoy embeddings similar to that pre-defined one only under this certain encoder. Further, when the encoder is changed, the embeddings of these samples will again become different. We named such kind of samples as *PEI attack samples* corresponding to the certain encoder, and they will be the key ingredient of our attack framework.

The idea is that for a targeted downstream service that is built upon this certain encoder, the corresponding PEI attack samples are very likely to make the downstream model produce a specific behavior determined by the pre-defined embedding. Besides, when the hidden encoder behind the targeted service is not the aforementioned certain encoder, such a specific behavior is less likely to be produced by the downstream model. Therefore, the adversary can exploit this behavior discrepancy to perform the PEI attack against downstream ML services. Such an idea is also illustrated in Figure 2, which includes examples of the PEI attack against image classification, text classification, and text-to-image generation.

A. General Framework

As explained before, finding PEI attack samples for different (candidate) encoders is a vital step in the PEI attack. In our attack framework, we propose to *synthesize* such attack

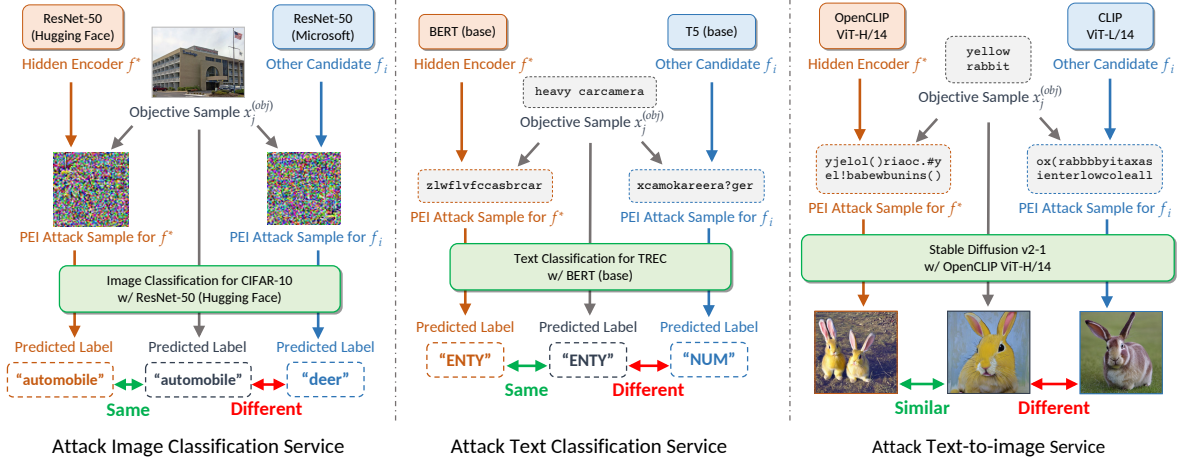


Fig. 2: Examples of the PEI attack against image classification service (ResNet-50 (Hugging Face) + CIFAR-10), text classification service (BERT (base) + TREC), and text-to-image generation service (StableDiffusion v2-1 with OpenCLIP ViT-H/14). The high-level attack idea is to first synthesize PEI attack samples that enjoy embeddings similar to that of a pre-defined objective sample, and then perform the inference attack by evaluating whether the synthesized attack samples can make downstream targeted service produce behaviors similar to that of the objective sample.

Algorithm 1 PEI Attack Framework

Input: Targeted downstream ML service g , candidate encoders f_1, \dots, f_N , objective samples $x_1^{(obj)}, \dots, x_{M_1}^{(obj)}$, Downstream service behavior similarity function ℓ_{sim} .

Output: Encoder \hat{f}^* inferred via the PEI attack.

- 1: // PEI Attack Samples Synthesis Stage
 - 2: **for** i **in** $1, \dots, N$ **do**
 - 3: Synthesize $\{x_{i,j,k}^{(atk)}\}_{k=1}^{M_2}$ via first randomly initializing them and then minimizing Eq. (1) based on $f_i, x_j^{(obj)}$, and a zeroth-order optimizer.
 - 4: **end for**
 - 5: // Hidden Encoder Inference Stage
 - 6: **for** i **in** $1, \dots, N$ **do**
 - 7: Calculate the PEI score ζ_i following Eq. (2) based on $g, f_i, \{x_j^{(obj)}\}_{j=1}^{M_1}$ and $\{x_{i,j,k}^{(atk)} : j \leq M_1, k \leq M_2\}$.
 - 8: **end for**
 - 9: Calculate z_1, \dots, z_N following Eq. (4).
 - 10: $I \leftarrow \{i : z_i > 1.7\}$
 - 11: **if** $|I| = 1$ **then**
 - 12: **return** $\hat{f}^* \leftarrow f_{i^*}$ $\triangleright i^*$ is the only element in set I .
 - 13: **end if**
 - 14: **return** $\hat{f}^* \leftarrow \emptyset$
-

samples for each encoder independently. This results in a two-stage PEI attack design: (1) **PEI attack samples synthesis stage**, and (2) **hidden encoder inference stage**. The overall implementation of the attack is presented as Algorithm 1. We now introduce the two stages in detail.

PEI attack samples synthesis stage. In this stage, the adversary first collects M_1 samples $x_1^{(obj)}, \dots, x_{M_1}^{(obj)}$ named *objective samples* from public data domains. Then, for each encoder-sample pair $(f_i, x_j^{(obj)})$ where $f_i \in E$ ($1 \leq i \leq N$) is the i -th candidate encoder and $x_j^{(obj)}$ ($1 \leq j \leq M_1$) is the j -th objective sample, the adversary synthesizes a set of

M_2 PEI attack samples $\{x_{i,j,k}^{(atk)}\}_{k=1}^{M_2}$. Each PEI attack sample $x_{i,j,k}^{(atk)}$ for the pair $(f_i, x_j^{(obj)})$ is first randomly initialized and then obtained via minimizing the following squared loss $\mathcal{L}_{i,j}$,

$$\mathcal{L}_{i,j}(x_{i,j,k}^{(atk)}) = \|f_i(x_{i,j,k}^{(atk)}) - f_i(x_j^{(obj)})\|_2^2. \quad (1)$$

Intuitively, Eq. (1) aims to make the embeddings of the PEI attack sample $x_{i,j,k}^{(atk)}$ and the objective sample $x_j^{(obj)}$ under the candidate encoder f_i similar to each other in ℓ_2 -distance. To minimize Eq. (1), a naive solution is to use gradient descent methods. However, since our threat model only assumes black-box access to the candidate encoder f_i , the adversary is not able to calculate first-order gradients of Eq. (1), which thus makes simple gradient descent methods become invalid. We skip this for now and will show how to tackle Eq. (1) via zeroth-order optimization [27, 26, 25] in Section V.

Hidden encoder inference stage. In this stage, for the pre-trained encoder f^* hidden in the targeted downstream ML service $g(\cdot) := h_\theta(f^*(\cdot))$, the adversary exploits the synthesized PEI attack samples to infer (1) whether $f^* \in E$ or not and (2) if so, which $f_i \in E$ is f^* . We argue that these two goals can be solved simultaneously. Concretely, we propose to first calculate N PEI scores ζ_1, \dots, ζ_N for the N candidates, where each ζ_i is calculated based on objective samples $x_1^{(obj)}, \dots, x_{M_1}^{(obj)}$ and PEI attack samples $\{x_{i,j,k}^{(atk)} : j \leq M_1, k \leq M_2\}$ corresponding to the candidate $f_i \in E$ as follows,

$$\zeta_i = \frac{1}{M_1 M_2} \sum_{j=1}^{M_1} \sum_{k=1}^{M_2} \ell_{sim}(g(x_{i,j,k}^{(atk)}), g(x_j^{(obj)})), \quad (2)$$

where $\ell_{sim} : \mathcal{Y} \times \mathcal{Y} \rightarrow \mathbb{R}^+$ is a task-dependent function that measures the similarity of behaviors produced by the targeted downstream service g . A larger output $\ell_{sim}(\cdot, \cdot)$ means the corresponding two inputs are more similar to each other. Then, among these N PEI scores ζ_1, \dots, ζ_N , if there happens to be a single PEI score, denoted as ζ_{i^*} , that is significantly higher than others, one can thus conclude that $f^* \in E$ and $f^* = f_{i^*}$,

otherwise conclude $f^* \notin E$. After that, the aforementioned two PEI attack goals have been accomplished.

Based on the above analysis, the remaining task to complete the PEI attack is to find a way to assess whether a given PEI score is truly significantly higher than others. Here we leverage a simple yet efficient *one-tailed z-test* to realize our goal. Specifically, for each PEI score ζ_i , if the candidate encoder f_i is not the hidden one f^* , then the score ζ_i would be relatively low. As a result, we can check whether ζ_i is significantly high by testing the following null hypothesis,

$$H_0^{(i)}: \text{The PEI score } \zeta_i \text{ is NOT calculated based on PEI attack samples for the hidden encoder } f^*. \quad (3)$$

If $H_0^{(i)}$ is rejected, then ζ_i will be determined to be significantly high and f_i will be inferred as the hidden f^* .

To use the one-tailed *z-test* to evaluate the null hypothesis, one needs to construct the following statistic *z-score*,

$$z_i = \frac{\zeta_i - \mathbb{E}[\zeta_{i'}]_{i'=1}^N}{\text{SD}[\zeta_{i'}]_{i'=1}^N}, \quad (4)$$

where $\mathbb{E}[\zeta_{i'}]_{i'=1}^N$ and $\text{SD}[\zeta_{i'}]_{i'=1}^N$ are the mean and the sample standard deviation of the N candidate PEI scores ζ_1, \dots, ζ_N . If the z_i is above a chosen threshold, then the null hypothesis $H_0^{(i)}$ will be rejected. We further assume that the distribution of PEI scores calculated based on non-hidden encoders' PEI attack samples can be approximated by a normal distribution. In this case, if we chose $z_i > 1.7$ as the rejection criterion, then it will lead to a one-sided *p-value*, which is also the false-positive rate, of 4.45%. Since such a *p-value* is smaller than the typical statistical significance level threshold (which is 5%), we thus set the criterion as $z_i > 1.7$, which eventually leads to the following inference attack,

$$\hat{f}^* = \begin{cases} f_{i^*} & (|\{i : z_i > 1.7\}| = 1 \text{ and } z_{i^*} > 1.7) \\ \emptyset & (\text{otherwise}) \end{cases}, \quad (5)$$

where \emptyset means that no candidate is inferred as the hidden encoder f^* by the PEI attack.

B. Discussions

Hyperparameters selection. There are three hyperparameters in the PEI attack framework, which are: (1) N the number of candidate encoders, (2) M_1 the number of objective samples, and (3) M_2 the number of PEI attack samples (per candidate encoder and objective sample). Increasing N will make the *z-test* in the inference stage of the PEI attack more robust while increasing M_1 and M_2 will make the calculated PEI scores more reliable. In our experiments (Sections VI, VII, and VIII), N is set as 6 or 7. We also empirically find that only setting M_1 to be 10 (for image encoders) or 20 (for text encoders) and M_2 to be 20 is enough to synthesize effective PEI attack samples to launch the attack.

Query budget. We here focus on analyzing the black-box query budget of synthesizing PEI attack samples for single candidates. According to Algorithm 1, such a query budget for a single candidate encoder is $\mathcal{O}(M_1 \cdot M_2 \cdot C)$, where $\mathcal{O}(C)$ is the query budget for solving Eq. (1), which will be discussed in Section V. Combining with the aforementioned practical settings of M_1 and M_2 leads to a query budget of at most

Algorithm 2 Black-box PEI Attack Sample Synthesis (via Solving Eq. (1)) for Image Encoder

Input: Candidate image encoder f_i , objective image sample $x_j^{(obj)}$, random sampling number S , perturbation radius $\epsilon > 0$, training iteration T , learning rate η .

Output: Synthesized PEI attack sample $x_{i,j,k}^{(atk)}$.

- 1: Initialize $x_{i,j,k}^{(atk)}$ with uniform distribution $\mathcal{U}[0, 1]^{\dim(\mathcal{X})}$.
 - 2: Denote $\mathcal{L}_{i,j}(x) := \|f_i(x) - f_i(x_j^{(obj)})\|_2^2$.
 - 3: **for** t **in** $1, \dots, T$ **do**
 - 4: Draw S directions $\mu_1, \dots, \mu_S \sim \mathbb{S}^{\dim(\mathcal{X})-1}$.
 - 5: Estimate gradient $\nabla_x \mathcal{L}_{i,j}(x_{i,j,k}^{(atk)})$ following Eq. (6) based on ϵ and μ_1, \dots, μ_S .
 - 6: Update synthesized sample with gradient normalization:
 - 7: $x_{i,j,k}^{(atk)} \leftarrow x_{i,j,k}^{(atk)} - \frac{\eta \cdot \nabla_x \mathcal{L}_{i,j}(x_{i,j,k}^{(atk)})}{\|\nabla_x \mathcal{L}_{i,j}(x_{i,j,k}^{(atk)})\|_\infty}$.
 - 8: Clip $x_{i,j,k}^{(atk)}$ into the range $[0, 1]^{\dim(\mathcal{X})}$.
 - 9: **end for**
 - 10: **return** $x_{i,j,k}^{(atk)}$
-

$\mathcal{O}(400 \cdot C)$. In Sections VI-B and VII-B, we will further show that such a query budget is cheap in terms of price.

Comparison with existing works. We acknowledge that the idea of synthesizing data of similar embeddings has also been adopted by [22] to design encoder watermarks that can be verified in downstream services. However, their method is only a watermarking method, while the PEI is a type of privacy attack against pre-trained encoders. It is also worth noting that [22] is a white-box protection that requires accessing full parameters of pre-trained encoders to inject watermarks, while our PEI attack is a black-box attack that can work as long as black-box accesses to candidate encoders and targeted downstream services are provided.

V. PEI ATTACKS ON DIFFERENT DATA-MODALITIES

This section presents detailed designs of the PEI attack against pre-trained encoders on different data modalities. Concretely, we will discuss how to solve Eq. (1) in Section IV-A via zero-order optimization to synthesize PEI attack samples for *image encoders* and *text encoders*.

A. Black-box Attack Samples Synthesis for Image Encoders

When the candidate encoders f_1, \dots, f_N are image encoders, the objective function $\mathcal{L}_{i,j}(x)$ in Eq. (1) can be seen as a continuous function concerning the input image x . Therefore, one can first leverage zeroth-order gradient estimation techniques [26, 27] to estimate the gradient of the objective function in a black-box manner and then use standard stochastic gradient optimization methods to solve Eq. (1). These techniques have also been widely adopted to attack black-box ML image models [50, 49].

In this work, we use the two-point zeroth-order gradient estimation [27, 26] method to solve Eq. (1) for the image encoder f_i . Specifically, for the objective function $\mathcal{L}_{i,j}(x)$ in

Eq. (1), its gradient $\nabla_x \mathcal{L}_{i,j}(x)$ can be estimated as

$$\nabla_x \mathcal{L}_{i,j}(x) \approx \frac{\dim(\mathcal{X})}{S} \sum_{s=1}^S \frac{\mathcal{L}_{i,j}(x + \epsilon \mu_s) - \mathcal{L}_{i,j}(x - \epsilon \mu_s)}{2\epsilon} \mu_s, \quad (6)$$

where S is the estimation random sampling number, $\epsilon > 0$ is the estimation perturbation radius, and μ_1, \dots, μ_S are i.i.d. random vectors in the same shape of \mathcal{X} drawn from the unit sphere $\mathbb{S}^{\dim(\mathcal{X})-1}$. Here, a larger sampling number S will result in a more accurate gradient estimation but a higher encoder querying budget, and vice versa. We further adopt l_∞ -norm gradient normalization during the optimization to relieve the difficulty of turning learning rate η (since now we can explicitly specify the maximum pixel updating values). The overall procedures of solving Eq. (1) for image encoders are presented as Algorithm 2.

Query budget. Combine Algorithm 2 with Algorithm 1, we have that the query budget of synthesizing PEI attack images is $\mathcal{O}(M_1 \cdot M_2 \cdot T \cdot 2S)$ per candidate encoder. Our experiments show that setting M_1, M_2 to $10 \sim 20$ and T, S to $100 \sim 200$ is enough to perform an effective PEI attack against image encoders. This results in an attack cost estimated based on real-world EaaS prices of only hundreds of dollars per candidate encoder (see Section VI-B).

B. Black-box Attack Samples Synthesis for Text Encoders

When the candidate encoders f_1, \dots, f_N are text encoders, minimizing the objective function $\mathcal{L}_{i,j}(x)$ in Eq. (1) becomes a discrete optimization problem since the input x is discrete text data. This prevents one from applying the previous zeroth-order gradient estimation to text encoders.

To this end, we generalize the beam-search-based adversarial text synthesis method by [25] from a white-box method to fit our black-box attack setting. Specifically, in our attack, the adversary will synthesize PEI attack texts of length $T > 0$ character by character. During the whole synthesis process, at most $K_1 > 0$ candidate attack texts will be retained. In the t -th synthesis step, for each candidate text sample of length $(t-1)$, the adversary will concatenate it with $K_2 > 0$ randomly sampled characters to construct K_2 new samples of length t . This will result in $(K_1 \times K_2)$ new text samples of length t at all. Then, the adversary will retain the K_1 samples from the $(K_1 \times K_2)$ ones with the smallest optimization losses (see Eq. (1)) to form the new candidate attack samples. The overall procedures of synthesizing PEI attack text samples via Eq. (1) are presented as Algorithm 3.

Comparison with [25]. The original beam-search attack [25] is designed against **white-box generative language models (GLMs)** and thus could not be applied to our attacks against **black-box text encoders**. This is mainly due to the fact that the original method requires access to the tokenizer of the targeted models, which, however, is not known to the PEI adversary. We tackle this issue by introducing a new beam-search sampling strategy that performs uniform sampling on a pre-defined character set. Besides, it is also worth noting that currently, our new Algorithm 3 can only synthesize gibberish texts while [25] can synthesize legible ones since it leverages the natural generative ability of the targeted GLMs. We believe

Algorithm 3 Black-box PEI Attack Sample Synthesis (via Solving Eq. (1)) for Text Encoder

Input: Candidate text encoder f_i , objective text sample $x_j^{(obj)}$, a character set C , beam-search hyperparameters K_1 and K_2 , PEI attack sample text length T .

Output: synthesized PEI attack sample $x_{i,j,k}^{(atk)}$.

```

1: Initialize an empty array arr.
2: Insert an empty text sequence to arr.
3: Denote  $\mathcal{L}_{i,j}(x) := \|f_i(x) - f_i(x_j^{(obj)})\|_2^2$ .
4: for  $t$  in  $1, \dots, T$  do
5:   Initialize two empty array arr' and scores.
6:   for  $x$  in arr do
7:     Uniformly randomly draw  $K_2$  character
        $c_1, \dots, c_{K_2}$  from  $C$  without replacement.
8:     for  $s$  in  $1, \dots, K_2$  do
9:       arr'.append( $x \oplus c_s$ )           ▷  $\oplus$  denotes
                                         concatenation.
10:      scores.append( $\mathcal{L}_{i,j}(x \oplus c_s)$ )
11:    end for
12:    arr  $\leftarrow$  Top- $K_1$ (arr', scores)   ▷ Select  $K_1$ 
                                         samples from arr' with lowest scores to form a new arr
13:  end for
14: end for
15: Initialize an empty array scores.
16: for  $x$  in arr do
17:   scores.append( $\mathcal{L}_{i,j}(x)$ )
18: end for
19:  $x_{i,j}^{(atk)} \leftarrow$  Top-1(arr, scores)   ▷ Select the sample from
                                         arr with the lowest score as the eventual output.
20: return  $x_{i,j}^{(atk)}$ 

```

by introducing additional GLMs, Algorithm 3 can be further improved to also synthesize legible PEI attack texts.

Query budget. Combine Algorithms 1 and 3, we know the query budget of synthesizing PEI attack texts is $\mathcal{O}(M_1 \cdot M_2 \cdot T \cdot K_1 \cdot K_2)$ per candidate. Our experiments show that setting $M_1, M_2 \leq 20$, $T \leq 32$, $K_1 \leq 200$, and $K_2 \leq 32$ is enough to perform an effective PEI attack against text encoders. This results in an estimated attack cost of hundreds of dollars per candidate encoder (see Sections VI-B and VII-B).

VI. EXPERIMENTS ON IMAGE AND TEXT CLASSIFICATIONS

This section empirically analyzes PEI attack against image or text encoders hidden in image or text classification services.

A. Experimental Setup

Downstream datasets. For image classification, we adopt four image datasets as the downstream data, which are: **CIFAR-10** [51], **SVHN** [52], **STL-10** [53], and **Food-101** [54]. For text classification, we adopt four text datasets as the downstream data, which are: **SST-5** [55], **Yelp** [56], **AG-News** [56], and **TREC** [57]. Please refer to Appendix A-A for more details about these datasets.

Pre-trained encoders. For image classification, six image encoders are adopted as candidates in the PEI attack.

TABLE I: PEI scores and PEI z -scores of candidate encoders on different downstream image classification services. If a candidate has z -score that is the only one above the threshold, then it is inferred as the encoder hidden in the downstream service.

| Downstream Task Dataset | Candidate Encoder | Candidate Encoder PEI Score (%) / PEI z -Score (Threshold = 1.7) | | | | | | Inferred Encoder | Attack Success |
|----------------------------|-------------------|--|---------------------|---------------------|---------------------|---------------------|---------------------|------------------|----------------|
| | | RN34 (HF) | RN50 (HF) | RN34 (MS) | RN50 (MS) | MobileNetV3 | CLIP ViT-L/14 | | |
| CIFAR-10 | RN34 (HF) | 74.50 / 2.04 | 3.00 / -0.33 | 0.00 / -0.43 | 0.00 / -0.43 | 1.00 / -0.40 | 0.00 / -0.43 | RN34 (HF) | ✓ |
| | RN50 (HF) | 11.50 / -0.46 | 57.50 / 1.98 | 10.50 / -0.52 | 22.00 / 0.09 | 10.50 / -0.52 | 9.50 / -0.57 | RN50 (HF) | ✓ |
| | RN34 (MS) | 39.50 / -0.38 | 40.00 / -0.34 | 78.00 / 2.03 | 36.50 / -0.56 | 39.50 / -0.38 | 39.50 / -0.38 | RN34 (MS) | ✓ |
| | RN50 (MS) | 2.00 / -0.56 | 15.50 / 0.03 | 0.50 / -0.62 | 60.50 / 1.99 | 3.50 / -0.49 | 7.00 / -0.34 | RN50 (MS) | ✓ |
| | MobileNetV3 | 0.00 / -0.41 | 0.50 / -0.39 | 0.00 / -0.41 | 0.00 / -0.41 | 59.50 / 2.04 | 0.00 / -0.41 | MobileNetV3 | ✓ |
| | CLIP ViT-L/14 | 20.00 / -0.41 | 20.00 / -0.41 | 20.00 / -0.41 | 20.00 / -0.41 | 20.00 / -0.41 | 57.50 / 2.04 | CLIP ViT-L/14 | ✓ |
| SVHN | RN34 (HF) | 75.00 / 2.03 | 15.50 / -0.41 | 16.00 / -0.39 | 15.00 / -0.43 | 20.50 / -0.20 | 11.00 / -0.59 | RN34 (HF) | ✓ |
| | RN50 (HF) | 28.50 / -0.52 | 64.00 / 2.03 | 30.50 / -0.38 | 32.00 / -0.27 | 30.50 / -0.38 | 29.00 / -0.49 | RN50 (HF) | ✓ |
| | RN34 (MS) | 23.00 / -0.07 | 15.00 / -0.58 | 55.00 / 1.95 | 15.00 / -0.58 | 24.50 / 0.02 | 12.50 / -0.74 | RN34 (MS) | ✓ |
| | RN50 (MS) | 20.50 / -0.21 | 19.00 / -0.40 | 21.50 / -0.08 | 35.50 / 1.74 | 24.00 / 0.25 | 12.00 / -1.31 | RN50 (MS) | ✓ |
| | MobileNetV3 | 18.50 / -0.92 | 20.50 / -0.16 | 21.00 / 0.03 | 19.50 / -0.54 | 26.00 / 1.93 | 20.00 / -0.35 | MobileNetV3 | ✓ |
| | CLIP ViT-L/14 | 10.50 / -0.32 | 9.00 / -0.46 | 9.00 / -0.46 | 10.50 / -0.32 | 9.00 / -0.46 | 36.00 / 2.04 | CLIP ViT-L/14 | ✓ |
| STL-10 | RN34 (HF) | 88.50 / 2.04 | 49.00 / -0.43 | 49.50 / -0.40 | 50.00 / -0.37 | 49.50 / -0.40 | 49.00 / -0.43 | RN34 (HF) | ✓ |
| | RN50 (HF) | 13.00 / -0.49 | 79.50 / 1.84 | 10.00 / -0.60 | 41.00 / 0.49 | 10.00 / -0.60 | 9.00 / -0.64 | RN50 (HF) | ✓ |
| | RN34 (MS) | 14.50 / -0.52 | 17.50 / -0.38 | 70.50 / 2.03 | 19.50 / -0.29 | 15.00 / -0.50 | 18.50 / -0.34 | RN34 (MS) | ✓ |
| | RN50 (MS) | 9.50 / -0.59 | 37.50 / 0.47 | 11.50 / -0.52 | 73.50 / 1.85 | 7.50 / -0.67 | 11.00 / -0.54 | RN50 (MS) | ✓ |
| | MobileNetV3 | 2.00 / -0.43 | 3.00 / -0.40 | 3.00 / -0.40 | 5.50 / -0.31 | 72.00 / 2.04 | 0.00 / -0.50 | MobileNetV3 | ✓ |
| | CLIP ViT-L/14 | 6.00 / -0.50 | 8.50 / -0.39 | 6.00 / -0.50 | 9.50 / -0.35 | 11.00 / -0.29 | 65.00 / 2.03 | CLIP ViT-L/14 | ✓ |
| Food-101 | RN34 (HF) | 43.50 / 2.04 | 0.00 / -0.41 | 0.00 / -0.41 | 0.00 / -0.41 | 0.00 / -0.41 | 0.00 / -0.41 | RN34 (HF) | ✓ |
| | RN50 (HF) | 1.00 / -0.38 | 27.50 / 2.04 | 0.50 / -0.43 | 1.50 / -0.33 | 0.50 / -0.43 | 0.00 / -0.47 | RN50 (HF) | ✓ |
| | RN34 (MS) | 0.00 / -0.41 | 0.00 / -0.41 | 25.00 / 2.04 | 0.00 / -0.41 | 0.00 / -0.41 | 0.00 / -0.41 | RN34 (MS) | ✓ |
| | RN50 (MS) | 0.50 / -0.36 | 0.00 / -0.44 | 0.00 / -0.44 | 15.00 / 2.04 | 0.50 / -0.36 | 0.00 / -0.44 | RN50 (MS) | ✓ |
| | MobileNetV3 | 0.00 / -0.41 | 0.00 / -0.41 | 0.00 / -0.41 | 0.00 / -0.41 | 24.50 / 2.04 | 0.00 / -0.41 | MobileNetV3 | ✓ |
| | CLIP ViT-L/14 | 0.00 / -0.41 | 0.00 / -0.41 | 0.00 / -0.41 | 0.00 / -0.41 | 0.00 / -0.41 | 9.50 / 2.04 | CLIP ViT-L/14 | ✓ |

They are: **ResNet-34 (HF)** [58], **ResNet-50 (HF)** [58], **MobileNetV3** [59], **ResNet-34 (MS)** [58], **ResNet-50 (MS)** [58], and (the vision encoder of) **CLIP ViT-L/14** [2]. The first three encoders are pre-trained by Hugging Face, the fourth and fifth ones are pre-trained by Microsoft, and the last one is pre-trained by OpenAI. Besides, for text classification, we also leverage six text encoders as the candidates, which are: **BERT (base)** [1], **BERT (large)** [1], **T5 (small)** [5], **T5 (base)** [5], **RoBERTa (base)** [60], and (the language encoder of) **CLIP ViT-L/14** [2]. The first four encoders are pre-trained by Google, the fifth one is pre-trained by Facebook, and the last one is pre-trained by OpenAI. These pre-trained image/text encoders can be downloaded from the Hugging Face Model Repository. See Table IX in Appendix C for details.

Building downstream services. For each pair of encoder and downstream dataset, we fix the encoder and train a downstream classifier based on embeddings of downstream training data obtained from the encoder. For each service, the downstream classifier is an MLP consisting of three fully-connected layers, where the dimension of each hidden layer is 512. We use Adam to train the classifier for 10,000 iterations, where the batch size is set as 512 and the learning rate is set as 0.001 and decayed by a factor of 0.1 every 4,000 iterations.

PEI attack image synthesis. For image encoders, we randomly select $M_1 = 10$ images from the PASCAL VOC 2012 dataset [61] as the objective samples $x_1^{(obj)}, \dots, x_{M_1}^{(obj)}$. They are collected and presented as Figure 13 in Appendix A-B. For each pair of candidate encoder f_i and objective sample $x_j^{(obj)}$, we follow Algorithm 2 to synthesize $M_2 = 20$ PEI attack images $x_{i,j,1}^{(atk)}, \dots, x_{i,j,M_2}^{(atk)}$. For the hyperparameters, without explicitly stating, the perturbation radius ϵ is set as 5.0, the

sampling number S is set as 100, the training iterations number T is set as 200, and the learning rate is fixed to 0.1. The shape of each synthesized PEI attack image is 64×64 .

PEI attack text synthesis. For text encoders we manually construct $M_1 = 20$ sentences as the objective texts $x_1^{(obj)}, \dots, x_{M_1}^{(obj)}$, where each sentence follows the structure $\{\text{Adjective}\} + \{\text{Noun}\}$. They are collected in Table V in Appendix A-B. For each pair of candidate encoder f_i and objective text $x_j^{(obj)}$, we follow Algorithm 3 to synthesize $M_2 = 20$ PEI attack texts $x_{i,j,1}^{(atk)}, \dots, x_{i,j,M_2}^{(atk)}$. For the hyperparameters, without explicitly stating, the character set is “abcdefghijklmnopqrstuvwxyz!?. ,”, the text length T is set as 16, and the beam-search parameters K_1 and K_2 are set as 150 and 16 respectively.

PEI score calculation. To calculate the PEI score ζ_i via Eq. (2), the adversary needs to have a task-dependent similarity function ℓ_{sim} . In this section, for classification tasks, we leverage the indicator function $1[\cdot]$ and calculate the PEI score as $\zeta_i = \frac{1}{M_1 M_2} \sum_{j=1}^{M_1} \sum_{k=1}^{M_2} 1[g(x_j^{(obj)}) = g(x_{i,j,k}^{(atk)})]$.

B. Results Analysis

Classification accuracies of the 24 built image classification services (6 image encoders \times 4 downstream image datasets) and the 24 built text classification services (6 text encoders \times 4 downstream text datasets) are reported as Table VI and Table VII in Appendix A-C. We next show how PEI attacks can reveal encoders hidden in these downstream targets.

The PEI attack is extremely effective against hidden image encoders. The PEI scores and PEI z -scores of candidate

TABLE II: PEI scores and PEI z -scores of candidate encoders on different downstream text classification services. If a candidate has z -score that is the only one above the threshold, then it is inferred as the encoder hidden in the downstream service.

| Downstream Task | | Candidate Encoder PEI Score (%) / PEI z -Score (Threshold = 1.7) | | | | | | Inferred Encoder | Attack Success |
|-----------------|----------------|--|---------------------|---------------------|---------------------|---------------------|---------------------|------------------|----------------|
| Dataset | Encoder | BERT (base) | BERT (large) | T5 (small) | T5 (base) | RoBERTa (base) | CLIP ViT-L/14 | | |
| SST-5 | BERT (base) | 38.50 / 1.92 | 22.50 / -0.01 | 21.50 / -0.13 | 20.50 / -0.25 | 15.00 / -0.91 | 17.25 / -0.64 | BERT (base) | ✓ |
| | BERT (large) | 28.25 / -0.31 | 43.75 / 2.02 | 27.25 / -0.46 | 29.25 / -0.16 | 26.25 / -0.61 | 27.00 / -0.49 | BERT (large) | ✓ |
| | T5 (small) | 33.25 / 0.11 | 31.50 / -0.79 | 35.75 / 1.38 | 31.50 / -0.79 | 35.00 / 1.00 | 31.25 / -0.91 | ∅ | ✗ |
| | T5 (base) | 38.50 / 0.14 | 38.75 / 0.21 | 35.25 / -0.77 | 38.50 / 0.14 | 33.25 / -1.33 | 43.75 / 1.60 | ∅ | ✗ |
| | RoBERTa (base) | 24.50 / -0.63 | 19.75 / -1.53 | 28.00 / 0.04 | 29.00 / 0.23 | 35.25 / 1.42 | 30.25 / 0.47 | ∅ | ✗ |
| | CLIP ViT-L/14 | 27.75 / -0.57 | 25.25 / -0.88 | 33.50 / 0.14 | 32.00 / -0.05 | 28.00 / -0.54 | 47.75 / 1.90 | CLIP ViT-L/14 | ✓ |
| TREC | BERT (base) | 63.75 / 2.00 | 30.00 / -0.39 | 27.00 / -0.60 | 30.25 / -0.37 | 35.00 / -0.04 | 27.00 / -0.60 | BERT (base) | ✓ |
| | BERT (large) | 35.25 / -0.13 | 50.25 / 1.35 | 43.75 / 0.71 | 33.25 / -0.32 | 36.50 / 0.00 | 20.25 / -1.60 | ∅ | ✗ |
| | T5 (small) | 12.00 / -1.16 | 10.50 / -1.27 | 43.75 / 1.18 | 37.00 / 0.68 | 32.25 / 0.33 | 31.00 / 0.24 | ∅ | ✗ |
| | T5 (base) | 22.75 / -1.33 | 29.00 / -0.47 | 34.00 / 0.21 | 45.00 / 1.71 | 32.75 / 0.04 | 31.25 / -0.17 | T5 (base) | ✓ |
| | RoBERTa (base) | 36.50 / -0.39 | 37.25 / -0.30 | 40.75 / 0.14 | 46.50 / 0.87 | 49.50 / 1.24 | 27.25 / -1.56 | ∅ | ✗ |
| | CLIP ViT-L/14 | 24.00 / -0.42 | 24.50 / -0.35 | 24.75 / -0.32 | 26.50 / -0.10 | 21.00 / -0.80 | 42.75 / 1.99 | CLIP ViT-L/14 | ✓ |
| Yelp | BERT (base) | 46.50 / 1.80 | 31.25 / -0.73 | 30.00 / -0.94 | 32.75 / -0.48 | 36.00 / 0.06 | 37.50 / 0.30 | BERT (base) | ✓ |
| | BERT (large) | 38.50 / -1.63 | 55.50 / 1.20 | 52.75 / 0.74 | 45.00 / -0.55 | 48.25 / -0.01 | 49.75 / 0.24 | ∅ | ✗ |
| | T5 (small) | 26.00 / -0.71 | 26.25 / -0.68 | 44.25 / 1.77 | 34.75 / 0.48 | 25.25 / -0.82 | 31.00 / -0.03 | T5 (small) | ✓ |
| | T5 (base) | 25.50 / 0.11 | 17.00 / -0.97 | 28.50 / 0.49 | 38.00 / 1.70 | 18.75 / -0.75 | 20.00 / -0.59 | T5 (base) | ✓ |
| | RoBERTa (base) | 26.00 / -0.88 | 26.25 / -0.81 | 29.75 / 0.16 | 27.75 / -0.39 | 35.75 / 1.84 | 29.50 / 0.09 | RoBERTa (base) | ✓ |
| | CLIP ViT-L/14 | 13.50 / -0.94 | 20.00 / -0.18 | 19.75 / -0.21 | 21.25 / -0.03 | 16.75 / -0.56 | 38.00 / 1.93 | CLIP ViT-L/14 | ✓ |
| AG-News | BERT (base) | 59.25 / 1.32 | 57.00 / 0.96 | 48.50 / -0.39 | 45.50 / -0.87 | 52.00 / 0.17 | 43.50 / -1.19 | ∅ | ✗ |
| | BERT (large) | 27.75 / -0.37 | 49.25 / 1.98 | 31.75 / 0.06 | 27.00 / -0.46 | 26.00 / -0.57 | 25.25 / -0.65 | BERT (large) | ✓ |
| | T5 (small) | 54.75 / 0.97 | 54.00 / 0.73 | 54.75 / 0.97 | 47.75 / -1.26 | 49.25 / -0.78 | 49.75 / -0.62 | ∅ | ✗ |
| | T5 (base) | 39.00 / -1.05 | 41.75 / -0.44 | 46.50 / 0.61 | 51.50 / 1.71 | 41.00 / -0.61 | 42.75 / -0.22 | T5 (base) | ✓ |
| | RoBERTa (base) | 84.75 / -0.77 | 86.25 / -0.13 | 89.25 / 1.17 | 85.50 / -0.45 | 89.50 / 1.27 | 84.00 / -1.10 | ∅ | ✗ |
| | CLIP ViT-L/14 | 40.50 / -0.77 | 45.00 / -0.13 | 47.00 / 0.15 | 39.50 / -0.92 | 44.50 / -0.20 | 59.00 / 1.87 | CLIP ViT-L/14 | ✓ |

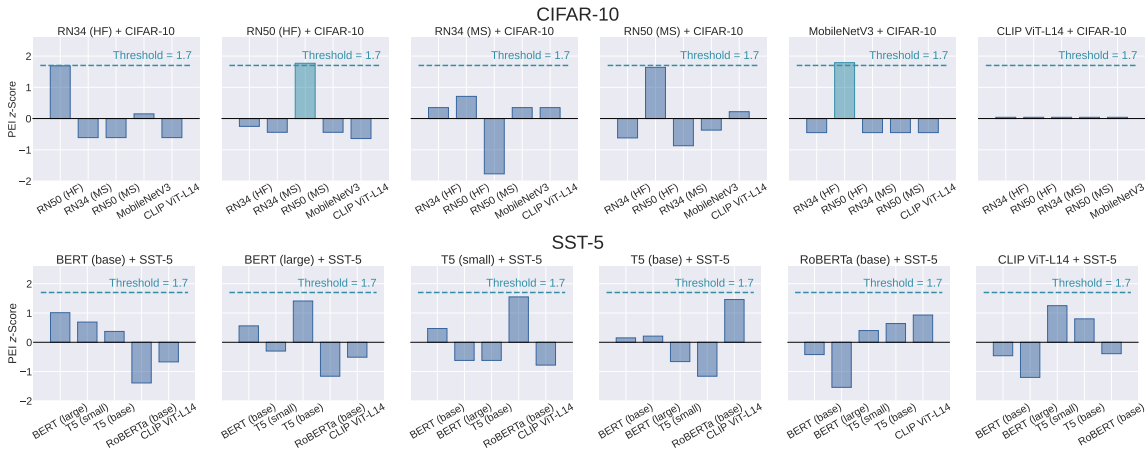


Fig. 3: PEI z -scores of candidate encoders on different CIFAR-10/SST-5 classification services where **the correct hidden encoder is not in the PEI candidates set**. z -scores that are above the preset threshold 1.7 are **highlighted**. Ideally, none of the reported z -score should go beyond the preset threshold.

image encoders in different image classification services are reported in Table I, which shows that our PEI attack succeeds in revealing hidden encoders in all 24 services. Specifically, in every attack case, the PEI z -score of the correct hidden encoder is always the only one that is above the preset threshold of 1.7 and in most cases, is around 2.0, which is significantly higher than the preset threshold. This indicates that the PEI attack is very confident in its (correct) predictions.

While the PEI attack is a bit less effective in revealing hidden text encoders, it is strong in avoiding false-positive inferences. For text classifications, the PEI scores and z -

scores of candidate text encoders are reported in Table II. In all the 24 downstream cases, the PEI attack correctly infers 14 hidden encoders, which, however, is less effective than that in image classifications. Further, in some failure cases, although the PEI score of the hidden encoder is the highest among all candidates, its corresponding z -score is not above the threshold 1.7 (e.g., RoBERTa (base) + SST-5) and thus resulted in failure. We deduce this is due to the fact that current synthesized PEI attack texts are gibberish, which makes them difficult to recognize by text encoders pre-trained on meaningful text data and thus could not enjoy semantic

embeddings similar to that of the human-readable objective texts (see Table V in Appendix A-B). A potential remedy is to improve the readability of synthesized PEI attack texts.

Nevertheless, it is also worth noting that the PEI attack **does not make false-positive inferences at all** against text encoders. In every failure case in Table II, the inferred result of the PEI attack is simply “ \emptyset ” (which means no significant candidate is found) rather than a wrong candidate encoder. Such a capability of avoiding false-positive inferences is very useful to adversaries, as they would thus not need to make meaningless efforts in tackling false-positive signals. It enables a PEI adversary to try many targets quickly and thus will have a good chance of finding a victim among them in a short time.

The PEI attack seldom makes mistakes when the targeted hidden encoder is not included in the candidate set. We now turn to analyzing the PEI attack in a more challenging setting where the targeted hidden encoder is not in the candidate set. We take the CIFAR-10 dataset for image classifications and the SST-5 dataset for text classifications as examples. In each case, we remove the correct hidden encoder from the candidates set and then launch the PEI attack following Algorithm 1 as usual with the remaining candidates. The z -scores of different candidates are presented as Figure 3.

Ideally, since the correct hidden encoder is excluded from the candidate set, all z -scores of remaining candidates should not go beyond the preset threshold 1.7 as none of these candidates are correct. From Figure 3, we find that the PEI attack only makes mistakes in inferring out incorrect candidates in 2 out of 6 cases on CIFAR-10 (*i.e.*, RN50 (HF) and MobileNetV3), and makes all correct inferences (*i.e.*, returning “ \emptyset ”) on SST-5. Combined with Table II, all results demonstrate that the PEI attack enjoys a strong and robust capability in avoiding false-positive inferences.

Query budget prices of both image and text encoders can be as low as hundreds of dollars. For image encoders, based on the query budget equation in Section V-A, the exact budget in this part of the experiments is 4 million per image encoder. According to Table VIII in Appendix D, the price of commonly used real-world EaaS for images is usually around \$0.0001 per image. Thus, the estimated price of synthesizing PEI attack images would be no more than \$400 per encoder.

Besides, for text encoders, based on the query budget equation in Section V-B the exact budget in this part of the experiments is no more than 15.4 million per text encoder. According to Table VIII in Appendix D, the price of commonly used real-world EaaS for texts is at most \$0.014 per 1,000 queries or \$0.1 per 1 million characters, which thus means the estimated price of synthesizing PEI attack texts in this section is an acceptable price of no more than \$215 per encoder.

C. Ablation Studies

Effect of downstream classifier initialization. The PEI attack in Tables I and II is conducted against single downstream classifiers. Yet, it remains unknown how the PEI attack would be affected by the random initialization of these classifiers. To investigate this, we conduct case studies on CIFAR-10 and SVHN datasets for image classification services and SST-5 and TREC datasets for text classification services. For each dataset-encoder pair, we retrain 5 downstream models, perform the PEI

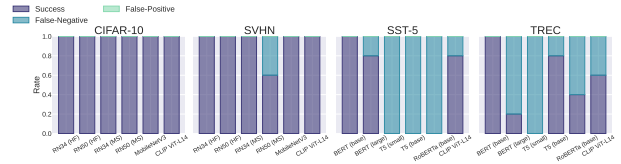


Fig. 4: Rates of different PEI attack results on CIFAR-10, SVHN, SST-5, and TREC datasets. Rates of **attack success**, **false-negative**, and **false-positive** are colored in different colors.

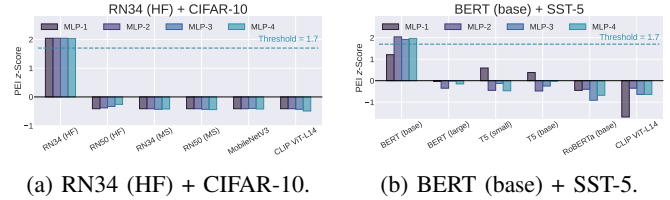


Fig. 5: PEI z -scores of candidates on classification services built with downstream classifiers of 4 different architectures. z -scores associated with different services are in different colors.

attack against all of them, and report rates of attack success, false-negative, and false-positive in Figure 4. This leads to a total of 24 analyzed cases.

From the figure, we have two observations. Firstly, PEI attacks never made false-positive inferences in all analyzed cases. As explained in the previous section, this capability is useful for PEI adversaries to quickly find victims from a large number of targeted services. Secondly, in most of the cases (except three cases “RN50 (MS) + SVHN”, “RoBERTa (base) + TREC”, and “CLIP ViT-L/14 + TREC”), the attack achieved consistent results, *i.e.*, either attack success or false-positive, with a possibility of at least 80%, in 21 out of 24 analyzed cases. This suggests that the PEI attack is generally insensitive to the initialization of downstream classifiers in image/text classification services.

Effect of downstream classifier architectures. So far, the architecture of downstream classifiers used in image/text classification services is fixed to a 3-layer MLP with a width of 512. We now analyze how the architecture of this classifier would affect the PEI attack performance. The analysis is conducted on two cases: “RN34 (HF) + CIFAR-10” and “BERT (base) + SST-5”. For each analyzed case, we build classification services with the targeted encoder and four different downstream classifiers, which are MLP-1, MLP-2, MLP-3, and MLP-4. Here, “MLP- x ” denotes an MLP architecture of x layers, where dimensions of all hidden layers (if it has) are fixed to 512. The training of these downstream classifiers follows that described in Section VI-A. After that, we attack each service with PEI attack samples originally used in Section VI-B. PEI z -scores are reported in Figure 5.

From the figure, one can find that the downstream classifier architecture has little effect on attacks against vision services (*i.e.*, “RN34 (HF) + CIFAR-10”): the PEI z -scores of each candidate are almost the same across different downstream classifier architectures, and the PEI attacks can always reveal the correct hidden encoder. However, for language services

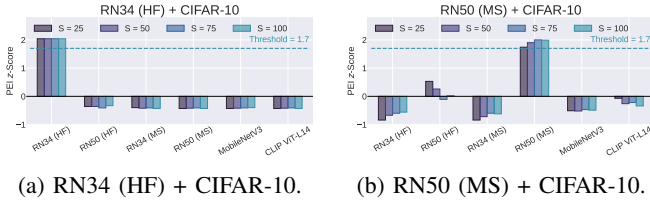


Fig. 6: PEI z -scores of candidates on image classification services with different gradient estimation sampling number S (see Algorithm 2) varies in $\{25, 50, 75, 100\}$.

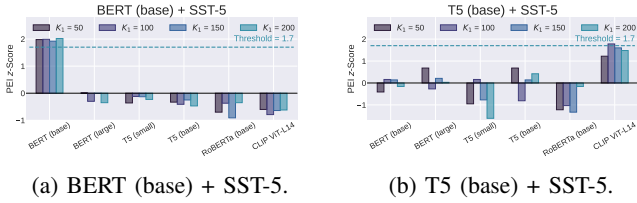


Fig. 7: PEI z -scores on text classification services with different beam-search parameter K_1 (see Algorithm 3) varies in $\{50, 100, 150, 200\}$.

(*i.e.*, “BERT (base) + SST-5”), PEI z -scores are significantly affected by downstream classifier architectures. In the worst case where the downstream classifier is MLP-1, the PEI attack even failed to infer the correct hidden encoder. Nevertheless, the PEI attack still succeeds in the remaining 3 cases.

Effect of zeroth-order gradient estimation. We now investigate how the zeroth-order gradient estimation in Algorithm 2 would affect the PEI attack against image encoders. Since the gradient estimation accuracy depends on the random sampling number S , we thus vary S in the set $\{25, 50, 75, 100\}$ (in Section VI-B, $S = 100$) to see how the attack performance would change. This study is conducted on “RN34 (HF) + CIFAR-10” and “RN50 (MS) + CIFAR-10”, and PEI z -scores of different encoders under different S are plotted in Figure 6. For the first case (Figure 6a), the sampling number S has little effect on PEI z -scores, while the z -score of the correct hidden encoder always stays in high level (around 2.0). For the second case (Figure 6b), one can find that as the sampling number S increases, the PEI z -score of the correct encoder significantly increases, while those of other candidates remain at low levels. These imply that when the PEI attack is weak, it can benefit from a large sampling number S . However, one should also notice that a large S would increase the query budget and the adversary needs to carefully trade-off between the utility and efficiency of the PEI attack.

Effect of beam-search-based optimization. Finally, we analyze how the improved black-box beam search (*i.e.*, Algorithm 3) would affect the PEI attack against text encoders. As the beam search only has two parameters, K_1 and K_2 , and we usually fix K_2 to be the half size of the character set C , here we only analyze the impact of K_1 on the PEI attack. The analysis is based on “T5 (base) + SST-5” and “BERT (base) + SST-5”, where the parameter K_1 varies in the set $\{50, 100, 150, 200\}$ and PEI z -scores on different encoders are plotted in Figure 7.

Intuitively, a high K_1 should lead to a strong PEI attack. However, from the figure, we find that as K_1 increases, the PEI scores of both correct and incorrect encoders change either slightly (Figure 7a) or without regular patterns (Figure 7b). We deduce this may be partially because current synthesized PEI texts are gibberish, and no matter how well the algorithm is for synthesizing gibberish, they are, in general, difficult to enjoy similar embeddings with those human-readable objective texts. Thus, improving the readability of PEI attack texts may also enhance the PEI attack. We leave this to future studies.

VII. EXPERIMENTS ON TEXT-TO-IMAGE GENERATION

This section empirically analyzes the PEI attack against text encoders hidden in real-world text-to-image services.

A. Experimental Setup

Pre-trained encoders. We adopt text encoders from six vision-language models to form the PEI candidate set. They are: **CLIP ViT-B/16** [2], **CLIP ViT-B/32**, **CLIP ViT-L/14**, **OpenCLIP ViT-B/32** [62], **OpenCLIP ViT-H/14**, and **OpenCLIP ViT-L/14**. All these pre-trained encoders can be downloaded from the Hugging Face Model Repository. See Table IX in Appendix C for details.

Downstream tasks. We directly use stable diffusion models [63] on the Hugging Face Model Repository as the downstream text-to-image generation task in our experiments (see Table IX in Appendix C for download links). They are: **Stable Diffusion-v1.2**, **Stable Diffusion-v1.4**, **Stable Diffusion-v2.1 (base)**, and **Stable Diffusion-v2.1**. The first two adopt the text encoder in CLIP ViT-L/14, while the last two adopt that in OpenCLIP ViT-H/14.

PEI attack samples synthesis. We use the same $K_1 = 20$ objective texts (see Table V in Appendix A-B) as that in text classification experiments. For each pair of objective text and candidate encoder, we synthesize $K_2 = 20$ PEI attack texts via Algorithm 3. For the chosen of hyperparameters, without explicitly stating, the character set C consists of all 26 lowercase alphabets, all 10 numbers, and additional characters “! ? . , ! @ # \$ % ^ & * () - = +”, the text length T as 32, and the beam-search parameters K_1 and K_2 are set as 64 and 32.

PEI score calculation. We use the image encoder in **CLIP ViT-B/16** to evaluate the behavior similarity in the PEI score calculation in Eq. (2). Concretely, for each pair of input objective and PEI attack texts, we first use the targeted text-to-image service to generate 4 pairs of images and then calculate the averaged cosine similarity of the 4 pairs of generated images. This leads to the PEI score calculation as

$$\zeta_i = \sum_{j,k,o=1}^{M_1, M_2, 4} \frac{\text{Cosine}(\text{CLIP}(g(x_j^{(obj)}))^{(o)}), \text{CLIP}((g_{i,j,k}^{(atk)}))^{(o)})}{4M_1M_2},$$

where $\text{Cosine}(\cdot, \cdot)$ is the cosine similarity function, CLIP denotes the image encoder in CLIP ViT-B/16, and $g(x_j^{(obj)})^{(o)}$ and $g(x_{i,j,k}^{(atk)})^{(o)}$ denote the o -th pair of generated images.

TABLE III: PEI scores and PEI z -scores of candidate encoders on different downstream text-to-image services. If a candidate has z -score that is the only one above the threshold, then it is inferred as the encoder hidden in the downstream service.

| Downstream Task | | Candidate Encoder PEI Score (%) / PEI z -Score (Threshold = 1.7) | | | | | | Inferred Encoder | Attack Success |
|-----------------|-----------------|--|---------------|--------------------|-----------------|-----------------|--------------------|------------------|----------------|
| Model | Text Encoder | CLIP ViT-B/16 | CLIP ViT-B/32 | CLIP ViT-L/14 | O-CLIP ViT-B/32 | O-CLIP ViT-L/14 | O-CLIP ViT-H/14 | | |
| SD-v1.2 | CLIP ViT-L/14 | 0.41 / -0.24 | 0.39 / -0.64 | 0.47 / 1.95 | 0.40 / -0.44 | 0.39 / -0.73 | 0.42 / 0.09 | CLIP ViT-L/14 | ✓ |
| SD-v1.4 | CLIP ViT-L/14 | 0.39 / -0.10 | 0.38 / -0.53 | 0.45 / 1.98 | 0.38 / -0.39 | 0.37 / -0.79 | 0.39 / -0.17 | CLIP ViT-L/14 | ✓ |
| SD-v2.1 | O-CLIP ViT-H/14 | 0.39 / -0.50 | 0.37 / -0.93 | 0.40 / -0.41 | 0.41 / -0.23 | 0.43 / 0.16 | 0.51 / 1.91 | O-CLIP ViT-H/14 | ✓ |
| SD-v2.1 (base) | O-CLIP ViT-H/14 | 0.39 / -0.50 | 0.37 / -0.91 | 0.39 / -0.50 | 0.40 / -0.12 | 0.41 / 0.11 | 0.50 / 1.91 | O-CLIP ViT-H/14 | ✓ |

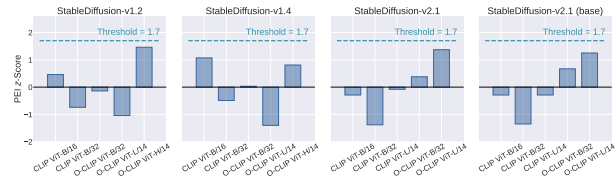
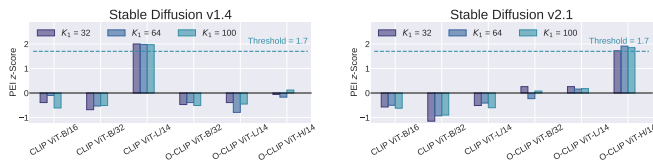


Fig. 8: PEI z -scores of candidate encoders on different text-to-image services where **the hidden encoder is not in the PEI candidates set**. No z -score go beyond the preset threshold (*i.e.*, 1.7) means that the attack makes no false-positive inference.



(a) Stable Diffusion v1.4. (b) Stable Diffusion v2.1.

Fig. 9: PEI z -scores on text-to-image services with different beam-search parameter K_1 (Algorithm 3) in $\{32, 64, 100\}$.

B. Results Analysis & Ablation Studies

Attack performance. PEI scores and z -scores of candidate text encoders on the four targeted downstream text-to-image models are reported in Table III, in which we find that the PEI attack succeeds in revealing hidden text encoders in all of the four targeted models. Additionally, in all cases, PEI z -scores of the correct candidates are around 1.9, which is significantly higher than the preset threshold 1.7. These results demonstrate that the PEI attack is very effective against text encoders in downstream text-to-image services.

The PEI attack does not make mistakes even when the targeted hidden encoder is excluded from the candidate set. For each of the 4 analyzed diffusion models, we remove its corresponding text encoder from the PEI candidates set and perform the PEI attack with the remaining candidates. The results are shown in Figure 8, from which we find that on all the 4 targeted services, no z -score of the incorrect remaining candidates is above the preset threshold 1.7. That means no incorrect candidate is inferred as the hidden encoders, and the PEI attack does not make a false-positive prediction in all analyzed attack scenarios.

Query budget in price. Based on the query budget equation in Section V-B, the exact budget in this part of the

experiments is no more than 26.5 million per text encoder. According to the pricing data collected in Table VIII in Appendix D, the price of commonly used real-world EaaS for texts is at most \$0.014 per 1,000 queries or \$0.1 per 1 million characters. This results in an acceptable price of synthesizing PEI attack texts of no more than \$370 per encoder.

Effect of beam-search-based optimization. Finally, we conduct an ablation study on the impact of the improved black-box beam search (*i.e.*, Algorithm 3) on the PEI attack against text encoders. Similar to that for text classification services (see Section VI-C), here we also focus on analyzing the beam search parameter K_1 (as K_2 is always fixed to be around the half size of the character set C). Specifically, the analysis is on the Stable Diffusion v1.4 and v2.1, where the parameter K_1 varies in the set $\{32, 64, 100\}$. From the figure, we find that keeping the K_1 to be sufficiently large (*e.g.*, set $K_1 = 64$ in Figure 9b) is necessary to ensure the PEI z -score of the correct hidden encoder is significantly above the preset threshold. However, further improving K_1 has little effect on the PEI attack performance but increases the query budget.

VIII. CASE STUDY: PEI-ASSISTED ADVERSARIAL ATTACKS AGAINST LLaVA

So far, we have justified the effectiveness of the PEI attack in revealing hidden encoders in downstream services through extensive experiments. In this section, we further show that the PEI attack itself is *useful*, by conducting a case study on how the PEI attack can assist adversarial attacks against LLaVA [28, 29], one of the most advanced multimodal models. Our results demonstrate there is indeed a need to design general defenses against the PEI attack.

Overview of LLaVA. The case study is based on the multimodal model LLaVA-1.5-13B [28], which is built upon a finetuned version of the Vicuna-1.5-13B language model [64] and the official version of the CLIP ViT-L/14-336px image encoder [2]. It takes images and texts as inputs and outputs texts, and thus can be used for multimodal tasks such as chatting or question-answering. Both of the LLaVA model and its CLIP image encoder can be downloaded from the Hugging Face model repository (see Table IX in Appendix C).

Overview of the attack. We consider an adversarial attack that aims to use **visually benign adversarial images** to induce LLaVA to generate **harmful information**. For instance, as shown in Figure 10, although the adversarial images only contain visually benign mosaics, LLaVA can read out misleading health/medical information from them. These adversarial images can be used to stealthily spread harmful information,

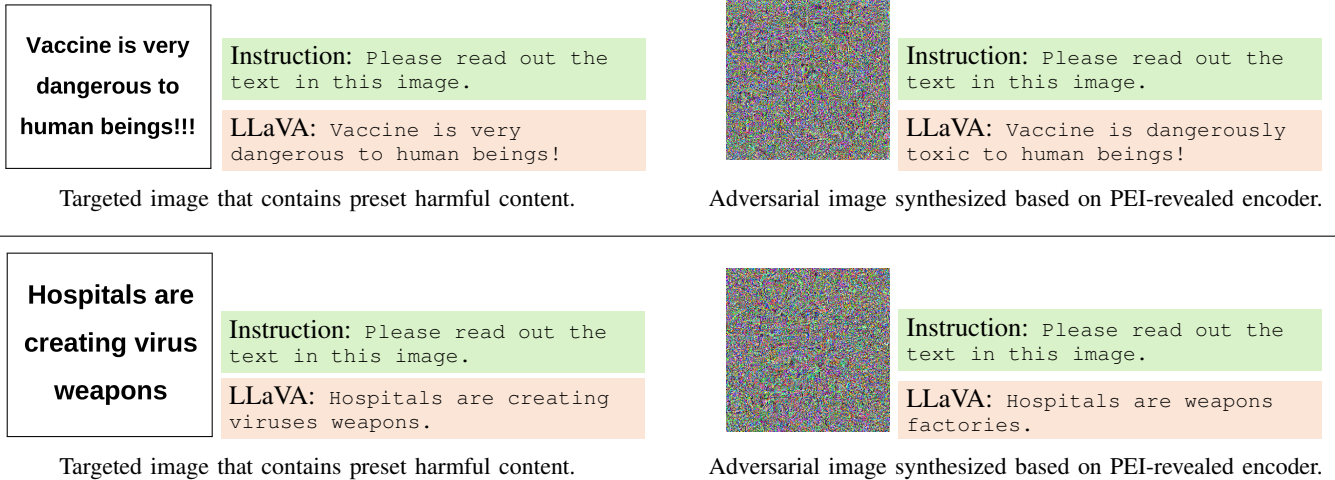


Fig. 10: Two examples of adversarial attacks against LLaVA with adversarial images synthesized based on the hidden image encoder revealed by the PEI attack. The synthesized adversarial images contain visually benign mosaics, but can induce LLaVA to generate predefined false health/medical information.

TABLE IV: PEI scores and z -scores of candidate image encoders on the LLaVA-v1.5-13b. If a candidate has z -score that is the only one above the threshold (*i.e.*, 1.7), then it is inferred as the encoder hidden in the downstream service.

| Candidate Image Encoder | PEI Score | PEI z -Score (Threshold = 1.7) |
|----------------------------|-------------|-------------------------------------|
| CLIP-ViT-B/16 | 0.55 | -1.50 |
| CLIP-ViT-B/32 | 0.64 | 0.22 |
| CLIP-ViT-L/14 | 0.60 | -0.46 |
| CLIP-ViT-L/14-336px | 0.72 | 1.76 |
| OpenCLIP-ViT-B/32 | 0.60 | -0.47 |
| OpenCLIP-ViT-L/14 | 0.65 | 0.45 |
| OpenCLIP-ViT-H/14 | 0.63 | 0.00 |

as their harmfulness is difficult for humans to detect. To launch such an adversarial attack with the assistance of the PEI attack, the adversary will first use the PEI attack to reveal the hidden image encoder (*i.e.*, CLIP-ViT-L/14-336px) used by LLaVA-1.5-13B. Then, the adversary will synthesize adversarial examples directly based on the hidden CLIP image encoder. We then discuss the two stages of the attack in detail.

Results of the PEI attack against LLaVA. We consider a PEI candidates set consists of seven image encoders, which are: **CLIP ViT-B/16** [2], **CLIP ViT-B/32**, **CLIP ViT-L/14**, **CLIP ViT-L/14-336px**, **OpenCLIP ViT-B/32** [62], **OpenCLIP ViT-H/14**, and **OpenCLIP ViT-L/14**. For the synthesis of PEI attack images, we adopt the same objective images and hyperparameters described in Section VI-A. For the PEI score calculation, to evaluate the behavior similarity in Eq. (2), we propose to leverage the question-answering capability of LLaVA to directly score the similarity between objective image and PEI attack images (in the range $[0, 1]$). See Appendix B-A for the detailed design of the PEI score calculation.

The PEI attack results are presented in Table IV, in which the correct hidden encoder, *i.e.*, CLIP ViT-L/14-336px, is the only one that enjoys a z -score above the preset threshold 1.7.

That means our PEI attack successfully reveals the image encoder hidden in LLaVA-1.5-13B.

Results of the PEI-assisted adversarial attack against LLaVA. After the image encoder (*i.e.*, CLIP ViT-L/14-336px) used by LLaVA-1.5-13B is revealed by the PEI attack, we then synthesize adversarial images that can induce LLaVA generating harmful contents solely based on the revealed image encoder. Specifically, as shown in Figure 2, to launch the attack, we first construct a targeted image that contains predefined harmful plain text content. Then, since the revealed hidden CLIP image encoder is an open-source model, we can synthesize an adversarial image by minimizing its embedding difference from that of the targeted image in a white-box manner. This will result in an adversarial image that contains benign mosaics but LLaVA can read out the predefined harmful content from it. Please refer to Appendix B-B for more details about the adversarial image synthesis.

We present two attack examples in Figure 2, in which one can find that LLaVA reads out false medical/health information from PEI-assisted adversarial images. This verifies the effectiveness of the PEI-assisted adversarial attack and further demonstrates the usefulness and hazards of the PEI attack.

IX. POTENTIAL DEFENSES

Finally, in this section, we discuss several potential defenses against the PEI attack.

A. Transforming PEI Attack Samples

A possible direction of defending the PEI attack is to perform data transformation on PEI attack samples before feeding them to the protected downstream service to sanitize their harmfulness. While many existing filtering-based methods [65, 66] could be used to remove malicious information in PEI attack samples, they may also reduce model performance on clean data. However, a series of works also focus on making adversarial examples robust to data transformation [67, 68,

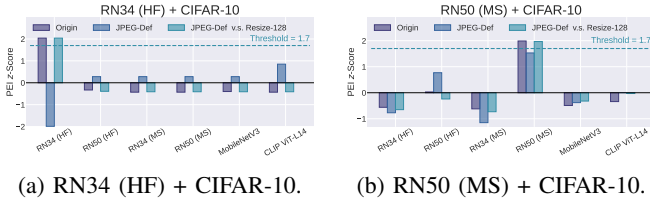


Fig. 11: PEI z -scores of candidates on image classification services. (1) “**Origin**”: original PEI attack results. (2) “**JPEG-Def**”: results of PEI attack against JPEG defense. (3) “**JPEG-Def v.s. Resize-128**”: results of PEI attack strengthened by image resizing (to shape 128×128) against JPEG defense.

69, 70]. Nevertheless, here we focus on analyzing two simple plug-and-play and downstream task-agnostic attack samples sanitizing methods for image and text encoders, respectively.

A plug-and-play preprocessing defense for image encoders. As PEI attack samples can somewhat be seen as adversarial examples [71], one may naturally seek to leverage defenses originally proposed for adversarial attacks to tackle the new PEI attack. As a preliminary investigation, here we adopt a task-agnostic and plug-and-play method named *JPEG defense* [72, 73] to protect downstream services from the PEI attack. Concretely, for each query image, the service supplier will first process it with the canonical JPEG compressing algorithm before feeding it into the real downstream service g . Since JPEG compression is found to be effective in destroying malicious information within adversarial images [72, 73], it may also be able to mitigate hazards of PEI attack images. A case study is conducted on two image classification services, “RN34 (HF) + CIFAR-10” and “RN50 (MS) + CIFAR-10”.

The results of JPEG defense against the vanilla PEI attack are presented in Figure 11, in which we plot z -scores of different candidates with and without the JPEG defense (denoted as “Origin” and “JPEG-Def” respectively). From the results, we find that the JPEG defense effectively defeats the PEI attack: in all cases, under the JPEG defense, the PEI z -scores of the correct hidden encoder are suppressed to low levels and no candidate goes beyond the preset threshold 1.7. However, we also discovered a simple method to bypass the JPEG defense for PEI attack: we just rescale each PEI attack image from 64×64 to 128×128 before sending them to the target service. Results are also presented in Figure 11 (denote as “JPEG-Def v.s. Resize-128”), which show that this rescaling approach enables the PEI attack to succeed again in all analyzed cases. We deduce the mechanism behind this is that resizing an attack image to a larger scale can prevent local features that contain malicious information from being compressed by JPEG defense.

A Plug-and-play preprocessing defense for text encoders. As a preliminary investigation, here we analyze a simple character-flipping defense. Specifically, for each input text, the service supplier will randomly select and flip a part of its characters to other (lowercase) alphabets before feeding it to the downstream service g . We conduct case studies on SST-5 with encoders BERT (base), BERT (large), and CLIP ViT-L/14, with a flipping proportion of 20%. In these three settings, the PEI attack originally succeeds in revealing the correct hidden

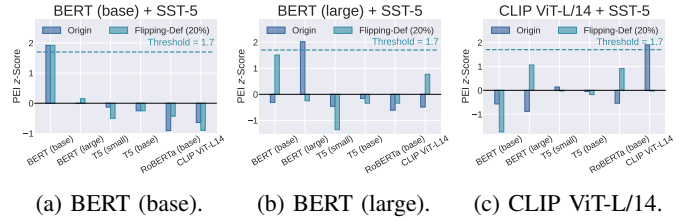


Fig. 12: PEI z -scores of candidates on SST-5 text classification services. (1) “**Origin**”: original PEI attack results. (2) “**Flipping-Def (20%)**”: results of PEI attack against character flipping defense (with a proportion of 20%).

encoders (see Table II). Results are presented as Figure 12, from which we find that while the random-flipping strategy effectively defeats the PEI attack in most settings, it could not always succeed (*e.g.*, in the case “BERT (base) + SST-5”). In addition, while a larger flipping proportion may improve the defense, it may also compromise the qualities of benign inputs.

B. Detecting PEI Attack Samples

Another direction of potential defenses is to leverage Out-of-distribution (OOD) detection methods to identify and drop malicious queries toward protected ML services. For image data, a series of detection methods [74, 75, 76, 77, 78] against adversarial images or backdoor images could be applied to defend against the PEI attack. For text data, it is found that perplexity filtering [79] can effectively identify gibberish but malicious texts from human-readable texts, while gibberish text is indeed used in PEI against text encoders.

However, PEI attack samples can also be made *stealth* to bypass potential detection defenses. For example, for image data, one may be able to exploit detection bypassing methods originally designed for adversarial images [80, 81, 82] to PEI attack images. For text data, by leveraging the strong natural language generation ability of LLMs, the adversary may further synthesize PEI attack texts that enjoy strong human-readability [69, 25, 83] and could thus be made to be robust to gibberish text detection-based defenses.

C. Architecture Resistance

More reliable defenses may be re-designing the pipeline of building downstream ML services to make them natively robust to the PEI attack. For example, since the current version of the PEI attack assumes that the targeted downstream service is built upon a single encoder, one may leverage multiple upstream encoders to build a single service to bypass the PEI attack. The idea of using multiple pre-trained encoders to build downstream models has already been adopted to improve the downstream model performance (*e.g.*, SDXL [84]). Our results suggest that apart from improving performance, there is also a great need to use multiple pre-trained encoders for the sake of downstream model security.

X. CONCLUSIONS

This paper unveils a novel privacy attack named *pre-trained encoder inference (PEI)* attack, which aims to reveal pre-trained encoders that are hidden in downstream ML services.

We design a general framework to perform the PEI attack in a black-box manner and further instantiate it for *image encoders* and *text encoders*. Extensive experiments on three downstream tasks, *i.e.*, image classification, text classification, and text-to-image generation, empirically verify the effectiveness of our new PEI attack. We further conduct a case study on a recent and advanced multimodal model, *i.e.*, LLaVA, to show the usefulness of the the PEI attack in assisting other ML attacks, such as adversarial attacks, against LLaVA. Results demonstrate the great need to design general defenses against the PEI attack. Additionally, we discuss several potential defenses against the PEI attack.

REFERENCES

- [1] J. Devlin, M.-W. Chang, K. Lee, and K. Toutanova, “BERT: Pre-training of deep bidirectional transformers for language understanding,” in *Proceedings of the 2019 Conference of the North American Chapter of the Association for Computational Linguistics: Human Language Technologies, Volume 1 (Long and Short Papers)*. Minneapolis, Minnesota: Association for Computational Linguistics, 2019, pp. 4171–4186.
- [2] A. Radford, J. W. Kim, C. Hallacy, A. Ramesh, G. Goh, S. Agarwal, G. Sastry, A. Askell, P. Mishkin, J. Clark *et al.*, “Learning transferable visual models from natural language supervision,” in *International Conference on Machine Learning*. PMLR, 2021, pp. 8748–8763.
- [3] K. He, H. Fan, Y. Wu, S. Xie, and R. Girshick, “Momentum contrast for unsupervised visual representation learning,” in *Proceedings of the IEEE/CVF Conference on Computer Vision and Pattern Recognition*, 2020, pp. 9729–9738.
- [4] Y. Xu, Q. Zhang, J. Zhang, and D. Tao, “ViTAE: Vision transformer advanced by exploring intrinsic inductive bias,” *Advances in Neural Information Processing Systems*, vol. 34, pp. 28 522–28 535, 2021.
- [5] C. Raffel, N. Shazeer, A. Roberts, K. Lee, S. Narang, M. Matena, Y. Zhou, W. Li, and P. J. Liu, “Exploring the limits of transfer learning with a unified text-to-text transformer,” *Journal of Machine Learning Research*, vol. 21, no. 140, pp. 1–67, 2020.
- [6] T. Chen, S. Kornblith, M. Norouzi, and G. Hinton, “A simple framework for contrastive learning of visual representations,” in *International Conference on Uachine Learning*. PMLR, 2020, pp. 1597–1607.
- [7] N. Carlini and A. Terzis, “Poisoning and backdooring contrastive learning,” in *International Conference on Learning Representations*, 2022.
- [8] H. Liu, J. Jia, and N. Z. Gong, “PoisonedEncoder: Poisoning the unlabeled pre-training data in contrastive learning,” in *31st USENIX Security Symposium (USENIX Security 22)*, 2022, pp. 3629–3645.
- [9] J. Jia, Y. Liu, and N. Z. Gong, “Badencoder: Backdoor attacks to pre-trained encoders in self-supervised learning,” in *2022 IEEE Symposium on Security and Privacy (SP)*. IEEE, 2022, pp. 2043–2059.
- [10] G. Tao, Z. Wang, S. Feng, G. Shen, S. Ma, and X. Zhang, “Distribution preserving backdoor attack in self-supervised learning,” in *2024 IEEE Symposium on Security and Privacy (SP)*. IEEE Computer Society, 2023, pp. 29–29.
- [11] Y. Wen, L. Marchyok, S. Hong, J. Geiping, T. Goldstein, and N. Carlini, “Privacy backdoors: Enhancing membership inference through poisoning pre-trained models,” *arXiv preprint arXiv:2404.01231*, 2024.
- [12] S. Feng and F. Tramèr, “Privacy backdoors: Stealing data with corrupted pretrained models,” *arXiv preprint arXiv:2404.00473*, 2024.
- [13] H. Liu, J. Jia, W. Qu, and N. Z. Gong, “EncoderMI: Membership inference against pre-trained encoders in contrastive learning,” in *Proceedings of the 2021 ACM SIGSAC Conference on Computer and Communications Security*, 2021, pp. 2081–2095.
- [14] X. He, H. Liu, N. Z. Gong, and Y. Zhang, “Semi-leak: Membership inference attacks against semi-supervised learning,” in *European Conference on Computer Vision*. Springer, 2022, pp. 365–381.
- [15] J. Zhu, J. Zha, D. Li, and L. Wang, “A unified membership inference method for visual self-supervised encoder via part-aware capability,” *arXiv preprint arXiv:2404.02462*, 2024.
- [16] Y. Liu, J. Jia, H. Liu, and N. Z. Gong, “StolenEncoder: Stealing pre-trained encoders in self-supervised learning,” in *Proceedings of the 2022 ACM SIGSAC Conference on Computer and Communications Security*, 2022, pp. 2115–2128.
- [17] Z. Sha, X. He, N. Yu, M. Backes, and Y. Zhang, “Can’t steal? Cont-steal! Contrastive stealing attacks against image encoders,” in *Proceedings of the IEEE/CVF Conference on Computer Vision and Pattern Recognition*, 2023, pp. 16 373–16 383.
- [18] A. Dziedzic, N. Dhawan, M. A. Kaleem, J. Guan, and N. Papernot, “On the difficulty of defending self-supervised learning against model extraction,” in *International Conference on Machine Learning*. PMLR, 2022, pp. 5757–5776.
- [19] S. L. Noorbakhsh, B. Zhang, Y. Hong, and B. Wang, “Inf2Guard: An information-theoretic framework for learning privacy-preserving representations against inference attacks,” *arXiv preprint arXiv:2403.02116*, 2024.
- [20] J. Dubiński, S. Pawlak, F. Boenisch, T. Trzcinski, and A. Dziedzic, “Bucks for buckets (B4B): Active defenses against stealing encoders,” vol. 36, 2023.
- [21] A. Tejankar, M. Sanjabi, Q. Wang, S. Wang, H. Firooz, H. Pirsiavash, and L. Tan, “Defending against patch-based backdoor attacks on self-supervised learning,” in *Proceedings of the IEEE/CVF Conference on Computer Vision and Pattern Recognition*, 2023, pp. 12 239–12 249.
- [22] P. Lv, P. Li, S. Zhu, S. Zhang, K. Chen, R. Liang, C. Yue, F. Xiang, Y. Cai, H. Ma, Y. Zhang, and G. Meng, “SSL-WM: A black-box watermarking approach for encoders pre-trained by self-supervised learning,” in *Network and Distributed System Security (NDSS) Symposium 2024*. San Diego, CA, USA: The Internet Society, 2024.
- [23] T. Cong, X. He, and Y. Zhang, “SSLGuard: A watermarking scheme for self-supervised learning pre-trained encoders,” in *Proceedings of the 2022 ACM SIGSAC Conference on Computer and Communications Security*. New York, NY, USA: Association for Computing Machinery, 2022, pp. 579–593.
- [24] A. Dziedzic, H. Duan, M. A. Kaleem, N. Dhawan, J. Guan, Y. Cattán, F. Boenisch, and N. Papernot, “Dataset inference for self-supervised models,” *Advances*

- in *Neural Information Processing Systems*, vol. 35, pp. 12 058–12 070, 2022.
- [25] V. S. Sadasivan, S. Saha, G. Sriramanan, P. Kattakinda, A. Chegini, and S. Feizi, “Fast adversarial attacks on language models in one GPU minute,” *arXiv preprint arXiv:2402.15570*, 2024.
- [26] J. C. Duchi, M. I. Jordan, M. J. Wainwright, and A. Wibisono, “Optimal rates for zero-order convex optimization: The power of two function evaluations,” *IEEE Transactions on Information Theory*, vol. 61, no. 5, pp. 2788–2806, 2015.
- [27] S. Liu, P.-Y. Chen, B. Kailkhura, G. Zhang, A. O. Hero III, and P. K. Varshney, “A primer on zeroth-order optimization in signal processing and machine learning: Principals, recent advances, and applications,” *IEEE Signal Processing Magazine*, vol. 37, no. 5, pp. 43–54, 2020.
- [28] H. Liu, C. Li, Y. Li, and Y. J. Lee, “Improved baselines with visual instruction tuning,” 2023.
- [29] H. Liu, C. Li, Q. Wu, and Y. J. Lee, “Visual instruction tuning,” in *Advances in Neural Information Processing Systems*, 2023.
- [30] R. Shokri, M. Stronati, C. Song, and V. Shmatikov, “Membership inference attacks against machine learning models,” in *2017 IEEE Symposium on Security and Privacy (SP)*. IEEE, 2017, pp. 3–18.
- [31] S. Yeom, I. Giacomelli, M. Fredrikson, and S. Jha, “Privacy risk in machine learning: Analyzing the connection to overfitting,” in *2018 IEEE 31st Computer Security Foundations Symposium (CSF)*. IEEE, 2018, pp. 268–282.
- [32] D. Chen, N. Yu, Y. Zhang, and M. Fritz, “GAN-leaks: A taxonomy of membership inference attacks against generative models,” in *Proceedings of the 2020 ACM SIGSAC Conference on Computer and Communications Security*, 2020, pp. 343–362.
- [33] N. Carlini, S. Chien, M. Nasr, S. Song, A. Terzis, and F. Tramèr, “Membership inference attacks from first principles,” in *2022 IEEE Symposium on Security and Privacy (SP)*. IEEE, 2022, pp. 1897–1914.
- [34] Z. Xiang, T. Wang, and D. Wang, “Preserving node-level privacy in graph neural networks,” in *2024 IEEE Symposium on Security and Privacy (SP)*. Los Alamitos, CA, USA: IEEE Computer Society, may 2024, pp. 198–198.
- [35] Z. Xiang, C. Wang, and D. Wang, “How does selection leak privacy: Revisiting private selection and improved results for hyper-parameter tuning,” *arXiv preprint arXiv:2402.13087*, 2024.
- [36] M. Fredrikson, S. Jha, and T. Ristenpart, “Model inversion attacks that exploit confidence information and basic countermeasures,” in *Proceedings of the 22nd ACM SIGSAC Conference on Computer and Communications Security*, 2015, pp. 1322–1333.
- [37] N. Carlini, F. Tramèr, E. Wallace, M. Jagielski, A. Herbert-Voss, K. Lee, A. Roberts, T. Brown, D. Song, U. Erlingsson *et al.*, “Extracting training data from large language models,” in *30th USENIX Security Symposium (USENIX Security 21)*, 2021, pp. 2633–2650.
- [38] J. Geiping, H. Bauermeister, H. Dröge, and M. Moeller, “Inverting gradients - How easy is it to break privacy in federated learning?” *Advances in Neural Information Processing Systems*, vol. 33, pp. 16 937–16 947, 2020.
- [39] F. Tramèr, R. Shokri, A. San Joaquin, H. Le, M. Jagielski, S. Hong, and N. Carlini, “Truth serum: Poisoning machine learning models to reveal their secrets,” in *Proceedings of the 2022 ACM SIGSAC Conference on Computer and Communications Security*, 2022, pp. 2779–2792.
- [40] B. Wang and N. Z. Gong, “Stealing hyperparameters in machine learning,” in *2018 IEEE Symposium on Security and Privacy (SP)*. IEEE, 2018, pp. 36–52.
- [41] D. Ippolito, N. Carlini, K. Lee, M. Nasr, and Y. W. Yu, “Reverse-engineering decoding strategies given blackbox access to a language generation system,” in *Proceedings of the 16th International Natural Language Generation Conference*. Prague, Czechia: Association for Computational Linguistics, 2023, pp. 396–406.
- [42] S. J. Oh, M. Augustin, M. Fritz, and B. Schiele, “Towards reverse-engineering black-box neural networks,” in *International Conference on Learning Representations*, 2018.
- [43] M. Finlayson, S. Swayamdipta, and X. Ren, “Logits of API-protected llms leak proprietary information,” *arXiv preprint arXiv:2403.09539*, 2024.
- [44] N. Carlini, D. Paleka, K. D. Dvijotham, T. Steinke, J. Hayase, A. F. Cooper, K. Lee, M. Jagielski, M. Nasr, A. Conmy, E. Wallace, D. Rolnick, and F. Tramèr, “Stealing part of a production language model,” in *International Conference on Machine Learning*, 2024.
- [45] D. Rolnick and K. Kording, “Reverse-engineering deep relu networks,” in *International Conference on Machine Learning*. PMLR, 2020, pp. 8178–8187.
- [46] M. Jagielski, N. Carlini, D. Berthelot, A. Kurakin, and N. Papernot, “High accuracy and high fidelity extraction of neural networks,” in *29th USENIX Security Symposium (USENIX Security 20)*, 2020, pp. 1345–1362.
- [47] F. Tramèr, F. Zhang, A. Juels, M. K. Reiter, and T. Ristenpart, “Stealing machine learning models via prediction APIs,” in *25th USENIX Security Symposium (USENIX Security 16)*, 2016, pp. 601–618.
- [48] T. Orekondy, B. Schiele, and M. Fritz, “Knockoff nets: Stealing functionality of black-box models,” in *Proceedings of the IEEE/CVF Conference on Computer Vision and Pattern Recognition*, 2019, pp. 4954–4963.
- [49] J.-B. Truong, P. Maini, R. J. Walls, and N. Papernot, “Data-free model extraction,” in *Proceedings of the IEEE/CVF Conference on Computer Vision and Pattern Recognition*, 2021, pp. 4771–4780.
- [50] S. Kariyappa, A. Prakash, and M. K. Qureshi, “MAZE: Data-free model stealing attack using zeroth-order gradient estimation,” in *Proceedings of the IEEE/CVF Conference on Computer Vision and Pattern Recognition*, 2021, pp. 13 814–13 823.
- [51] A. Krizhevsky, “Learning multiple layers of features from tiny images,” Tech. Rep., 2009.
- [52] Y. Netzer, T. Wang, A. Coates, A. Bissacco, B. Wu, A. Y. Ng *et al.*, “Reading digits in natural images with unsupervised feature learning,” in *NIPS Workshop on Deep Learning and Unsupervised Feature Learning*, vol. 2011, no. 5. Granada, Spain, 2011, p. 7.
- [53] A. Coates, A. Ng, and H. Lee, “An analysis of single-layer networks in unsupervised feature learning,” in *Proceedings of the Fourteenth International Conference on Artificial Intelligence and Statistics. JMLR Workshop and Conference Proceedings*, 2011, pp. 215–223.

- [54] L. Bossard, M. Guillaumin, and L. Van Gool, “Food-101 – Mining discriminative components with random forests,” in *European Conference on Computer Vision*. Springer International Publishing, 2014, pp. 446–461.
- [55] R. Socher, A. Perelygin, J. Wu, J. Chuang, C. D. Manning, A. Y. Ng, and C. Potts, “Recursive deep models for semantic compositionality over a sentiment treebank,” in *Proceedings of the 2013 Conference on Empirical Methods in Natural Language Processing*. Seattle, Washington, USA: Association for Computational Linguistics, 2013, pp. 1631–1642.
- [56] X. Zhang, J. Zhao, and Y. LeCun, “Character-level convolutional networks for text classification,” *Advances in Neural Information Processing Systems*, vol. 28, 2015.
- [57] E. M. Voorhees and D. M. Tice, “Building a question answering test collection,” in *Proceedings of the 23rd Annual International ACM SIGIR Conference on Research and Development in Information Retrieval*, ser. SIGIR ’00. New York, NY, USA: Association for Computing Machinery, 2000, p. 200–207.
- [58] K. He, X. Zhang, S. Ren, and J. Sun, “Deep residual learning for image recognition,” in *Proceedings of the IEEE Conference on Computer Vision and Pattern Recognition*, 2016, pp. 770–778.
- [59] A. Howard, M. Sandler, B. Chen, W. Wang, L.-C. Chen, M. Tan, G. Chu, V. Vasudevan, Y. Zhu, R. Pang, H. Adam, and Q. Le, “Searching for MobileNetV3,” in *2019 IEEE/CVF International Conference on Computer Vision (ICCV)*, 2019, pp. 1314–1324.
- [60] Y. Liu, M. Ott, N. Goyal, J. Du, M. Joshi, D. Chen, O. Levy, M. Lewis, L. Zettlemoyer, and V. Stoyanov, “RoBERTa: A robustly optimized bert pretraining approach,” *arXiv preprint arXiv:1907.11692*, 2019.
- [61] M. Everingham, L. Van Gool, C. K. I. Williams, J. Winn, and A. Zisserman, “The PASCAL Visual Object Classes Challenge 2012 (VOC2012) Results,” 2012.
- [62] M. Cherti, R. Beaumont, R. Wightman, M. Wortsman, G. Ilharco, C. Gordon, C. Schuhmann, L. Schmidt, and J. Jitsev, “Reproducible scaling laws for contrastive language-image learning,” in *Proceedings of the IEEE/CVF Conference on Computer Vision and Pattern Recognition*, 2023, pp. 2818–2829.
- [63] R. Rombach, A. Blattmann, D. Lorenz, P. Esser, and B. Ommer, “High-resolution image synthesis with latent diffusion models,” in *Proceedings of the IEEE/CVF Conference on Computer Vision and Pattern Recognition*, 2022, pp. 10 684–10 695.
- [64] L. Zheng, W.-L. Chiang, Y. Sheng, S. Zhuang, Z. Wu, Y. Zhuang, Z. Lin, Z. Li, D. Li, E. Xing *et al.*, “Judging LLM-as-a-judge with MT-bench and Chatbot arena,” *Advances in Neural Information Processing Systems Datasets and Benchmarks Track*, 2023.
- [65] F. Liao, M. Liang, Y. Dong, T. Pang, X. Hu, and J. Zhu, “Defense against adversarial attacks using high-level representation guided denoiser,” in *Proceedings of the IEEE Conference on Computer Vision and Pattern Recognition*, 2018, pp. 1778–1787.
- [66] W. Nie, B. Guo, Y. Huang, C. Xiao, A. Vahdat, and A. Anandkumar, “Diffusion models for adversarial purification,” in *International Conference on Machine Learning*. PMLR, 2022, pp. 16 805–16 827.
- [67] A. Athalye, L. Engstrom, A. Ilyas, and K. Kwok, “Synthesizing robust adversarial examples,” in *International Conference on Machine Learning*. PMLR, 2018, pp. 284–293.
- [68] S. Fu, F. He, Y. Liu, L. Shen, and D. Tao, “Robust unlearnable examples: Protecting data privacy against adversarial learning,” in *International Conference on Learning Representations*, 2022.
- [69] X. Liu, N. Xu, M. Chen, and C. Xiao, “Generating stealthy jailbreak prompts on aligned large language models,” in *International Conference on Learning Representations*, 2024.
- [70] Z. Chen, B. Li, S. Wu, K. Jiang, S. Ding, and W. Zhang, “Content-based unrestricted adversarial attack,” *Advances in Neural Information Processing Systems*, vol. 36, 2023.
- [71] I. Goodfellow, J. Shlens, and C. Szegedy, “Explaining and harnessing adversarial examples,” in *International Conference on Learning Representations*, 2015.
- [72] C. Guo, M. Rana, M. Cisse, and L. Van Der Maaten, “Countering adversarial images using input transformations,” *arXiv preprint arXiv:1711.00117*, 2017.
- [73] G. K. Dziugaite, Z. Ghahramani, and D. M. Roy, “A study of the effect of jpg compression on adversarial images,” *arXiv preprint arXiv:1608.00853*, 2016.
- [74] B. Tran, J. Li, and A. Madry, “Spectral signatures in backdoor attacks,” in *Advances in Neural Information Processing Systems*, vol. 31. Curran Associates, Inc., 2018.
- [75] T. Pang, C. Du, Y. Dong, and J. Zhu, “Towards robust detection of adversarial examples,” *Advances in Neural Information Processing Systems*, vol. 31, 2018.
- [76] Y. Dong, X. Yang, Z. Deng, T. Pang, Z. Xiao, H. Su, and J. Zhu, “Black-box detection of backdoor attacks with limited information and data,” in *Proceedings of the IEEE/CVF International Conference on Computer Vision*, 2021, pp. 16 482–16 491.
- [77] X. Li and F. Li, “Adversarial examples detection in deep networks with convolutional filter statistics,” in *Proceedings of the IEEE International Conference on Computer Vision*, 2017, pp. 5764–5772.
- [78] K. Roth, Y. Kilcher, and T. Hofmann, “The odds are odd: A statistical test for detecting adversarial examples,” in *International Conference on Machine Learning*. PMLR, 2019, pp. 5498–5507.
- [79] G. Alon and M. Kamfonas, “Detecting language model attacks with perplexity,” *arXiv preprint arXiv:2308.14132*, 2023.
- [80] O. Bryniarski, N. Hingun, P. Pachuca, V. Wang, and N. Carlini, “Evading adversarial example detection defenses with orthogonal projected gradient descent,” in *International Conference on Learning Representations*, 2022.
- [81] N. Carlini and D. Wagner, “Adversarial examples are not easily detected: Bypassing ten detection methods,” in *Proceedings of the 10th ACM workshop on Artificial Intelligence and Security*, 2017, pp. 3–14.
- [82] D. Hendrycks, K. Zhao, S. Basart, J. Steinhardt, and D. Song, “Natural adversarial examples,” in *Proceedings of the IEEE/CVF Conference on Computer Vision and Pattern Recognition*, 2021, pp. 15 262–15 271.
- [83] X. Xu, K. Kong, N. Liu, L. Cui, D. Wang, J. Zhang, and M. Kankanhalli, “An LLM can fool itself: A prompt-based adversarial attack,” in *International Conference on*

Learning Representations, 2024.

[84] D. Podell, Z. English, K. Lacey, A. Blattmann, T. Dockhorn, J. Müller, J. Penna, and R. Rombach, “Sdxl: Improving latent diffusion models for high-resolution image synthesis,” *arXiv preprint arXiv:2307.01952*, 2023.

APPENDIX A

ADDITIONAL EXPERIMENT DETAILS IN SECTION VI

A. Details of Datasets

1) *Downstream Datasets for Image Classification*: Four image datasets are used as the downstream data. They are: **CIFAR-10** [51] that consists of 50,000 training images and 10,000 test images from 10 classes; **STL-10** [53] that consists of 5,000 training images and 8,000 test images from 10 classes; **SVHN** [52] that consists of 73,257 training images and 26,032 test images from 10 classes; and **Food-101** [54] that consists of 75,750 training images and 25,250 validation images (used as test data) from 101 classes.

2) *Downstream Datasets for Text Classification*: Four text datasets are used as the downstream data. They are: **SST-5** [55] consists of 8,544 training sentences and 1,101 validation sentences (used as test data) from 5 classes; **Yelp** [56] consists of 650,000 training sentences and 50,000 test sentences from 5 classes; **AG-News** [56] consists of 120,000 training sentences and 7,600 test sentences from 4 classes; and **TREC** [57] consists of 5,452 training sentences and 500 test sentences from 6 classes.

B. Objective Samples in the PEI Attack

1) *Objective Images*: For the PEI attack against image encoders, we randomly sampled 10 images from the PASCAL VOC 2012 dataset [61] as the objective image samples. They are presented in Figure 13.

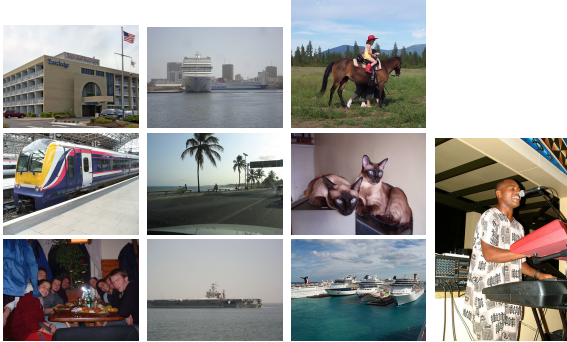


Fig. 13: The 10 objective images used in the PEI attack against image encoders.

2) *Objective Texts*: For the PEI attack against text encoders, we manually constructed 20 sentences following the template {Adjective} + {Noun} as the objective text samples. They are listed in Table V.

C. Downstream utilities of classification tasks

We collect and present the classification accuracy of downstream image/text classification services built on different

TABLE V: The 20 objective texts used in the PEI attack against text encoders.

| | | | |
|----|-----------------|-------------------|----|
| 1 | black bridge | red sunflower | 11 |
| 2 | dark battery | dirty battery | 12 |
| 3 | orange cherry | black mobilephone | 13 |
| 4 | yellow rabbit | heavy carcamera | 14 |
| 5 | white network | green aircraft | 15 |
| 6 | hot fish | muddy album | 16 |
| 7 | dirty softdrink | purple network | 17 |
| 8 | green album | hot house | 18 |
| 9 | beautiful oven | yellow bridge | 19 |
| 10 | purple dragon | ice opera | 20 |

TABLE VI: Test accuracy (%) of downstream image classification services built upon different pre-trained encoders.

| Downstream Dataset | Upstream Pre-trained Encoder | | | | | |
|--------------------|------------------------------|-----------|-----------|-----------|----------|---------------|
| | RN34 (HF) | RN50 (HF) | RN34 (MS) | RN50 (MS) | MobileV3 | CLIP ViT-L/14 |
| CIFAR-10 | 91.24 | 91.88 | 90.44 | 91.05 | 91.34 | 98.11 |
| SVHN | 62.93 | 67.22 | 60.99 | 69.67 | 71.23 | 82.58 |
| STL-10 | 97.16 | 97.86 | 96.74 | 97.92 | 96.44 | 99.83 |
| Food-101 | 64.40 | 68.66 | 63.26 | 68.67 | 71.20 | 94.66 |

TABLE VII: Test accuracy (%) of downstream text classification services built upon different pre-trained encoders.

| Downstream Dataset | Downstream Pre-trained Encoder | | | | | |
|--------------------|--------------------------------|--------------|------------|-----------|----------------|---------------|
| | BERT (base) | BERT (large) | T5 (small) | T5 (base) | RoBERTa (base) | CLIP ViT-L/14 |
| SST-5 | 40.51 | 43.14 | 40.69 | 43.42 | 43.87 | 39.15 |
| TREC | 92.20 | 85.00 | 93.40 | 94.40 | 94.00 | 91.80 |
| Yelp | 51.20 | 46.52 | 55.28 | 59.86 | 60.00 | 55.08 |
| AG-News | 89.46 | 79.71 | 91.39 | 93.07 | 93.30 | 93.07 |

downstream data and pre-trained encoders. The results of downstream image classification services are reported in Table VI, while those of downstream text classification services are reported in Table VII.

APPENDIX B

ADDITIONAL EXPERIMENT DETAILS IN SECTION VIII

A. PEI Score Calculation

To calculate PEI scores following Eq. (2), one has to carefully design how to calculate the behavior similarity $\ell_{sim}(g(x_{i,j,k}^{(atk)}), g(x_j^{(obj)}))$ between PEI attack image $x_{i,j,k}^{(atk)}$ and $x_j^{(obj)}$ for the LLaVA model g . To this end, we propose calculating the behavior similarity by directly questioning LLaVA about the similarity between objective and attack images (in the range $[0, 1]$). Specifically, we ask LLaVA with the following prompt template:

```
USER: <image>\n<image>\nScore the similarity (in the range [0,1], higher score means more similar) of the given two images\nASSISTANT:
```

where the two “<image>” in the prompt are placeholders for input images. We then construct the function $\ell_{ask}(\cdot, \cdot) : \mathcal{X} \times \mathcal{X} \rightarrow [0, 1]$ that maps the two (ordered) images to a similarity

TABLE VIII: Pricing data of common real-world EaaSs.

| Type | Supplier | Model Name | Price | Link |
|---------------|-------------------------|------------------------|--------------------------------|--|
| Image Encoder | Vertex AI (by Google) | multimodalembdings | \$0.0001 / Image Input | https://cloud.google.com/vertex-ai/generative-ai/pricing Accessed Date: 2024-04 |
| | Azure AI (by Microsoft) | Image Embeddings | \$0.10 / 1,000 Transactions | https://azure.microsoft.com/en-us/pricing/details/cognitive-services/computer-vision/ Accessed Date: 2024-04 |
| | OpenAI | text-embedding-3-small | \$0.02 / 1M Tokens | https://openai.com/pricing Accessed Date: 2024-04 |
| | OpenAI | text-embedding-3-large | \$0.13 / 1M Tokens | https://openai.com/pricing Accessed Date: 2024-04 |
| | OpenAI | ada v2 | \$0.10 / 1M Tokens | https://openai.com/pricing Accessed Date: 2024-04 |
| Text Encoder | Vertex AI (by Google) | multimodalembdings | \$0.0002 / 1K Characters Input | https://cloud.google.com/vertex-ai/generative-ai/pricing Accessed Date: 2024-04 |
| | Azure AI (by Microsoft) | Text Embeddings | \$0.014 / 1,000 Transactions | https://azure.microsoft.com/en-us/pricing/details/cognitive-services/computer-vision/ Accessed Date: 2024-04 |

score based on LLaVA and the above prompt. The eventual similarity function ℓ_{sim} in Eq. (2) is defined as follows,

$$\ell_{sim}(g(x_{i,j,k}^{(atk)}), g(x_j^{(obj)})) := \frac{1}{2} \left(\ell_{ask}(x_{i,j,k}^{(atk)}, x_j^{(obj)}) + \ell_{ask}(x_j^{(obj)}, x_{i,j,k}^{(atk)}) \right).$$

B. PEI-assisted Adversarial Example Synthesis

To synthesize adversarial examples based on the PEI-revealed image encoder (*i.e.*, CLIP ViT-L/14-336px), we propose to minimize their embedding difference with that of a targeted image containing preset harmful text content. Specifically, we aim to minimize the squared loss defined by embeddings of the adversarial image and targeted image. Since the hidden CLIP model is an open-source model, one can further leverage first-order gradient descent to optimize the objective squared loss. We use sign gradient to minimize the objective loss for 2,000 iterations, in which the learning rate is fixed to 0.01. Besides, to further improve the success rate of obtaining valid PEI-assisted adversarial images, for each targeted image, we will first synthesize 16 *candidate* adversarial images, and then choose a single image that enjoys the best attack performance among them as the eventual output.

APPENDIX C

PRE-TRAINED MODELS DOWNLOAD LINKS

All pre-trained encoders and downstream models in our experiments are available on the Hugging Face Model Repository. We list the download links to these models in Table IX.

APPENDIX D

PRICES OF ENCODER-AS-A-SERVICE IN THE WILD

To better estimate the cost of conducting PEI attacks in the wild, here we collect and list the prices of some common real-world EaaS in Table VIII. Combined with analyses in Sections VI-B and VII-B, the estimated price of the PEI attack is no more than \$400 per encoder.

TABLE IX: Download links of all pre-trained encoders and downstream models adopted in our experiments.

| Model Type | Name | Link |
|---------------------|----------------------------|---|
| Image Encoder | ResNet-34 (HF) | https://huggingface.co/imm/resnet34.a1_in1k |
| | ResNet-50 (HF) | https://huggingface.co/imm/resnet50.a1_in1k |
| | ResNet-34 (MS) | https://huggingface.co/microsoft/resnet-34 |
| | ResNet-50 (MS) | https://huggingface.co/microsoft/resnet-50 |
| | MobileNetV3 | https://huggingface.co/imm/mobilenetv3_large_100_ra_in1k |
| Text Encoder | BERT (base) | https://huggingface.co/google-bert/bert-base-uncased |
| | BERT (large) | https://huggingface.co/google-bert/bert-large-uncased |
| | T5 (small) | https://huggingface.co/google-t5/t5-small |
| | T5 (base) | https://huggingface.co/google-t5/t5-base |
| | RoBERTa (base) | https://huggingface.co/facebookAI/roberta-base |
| CLIP Model | CLIP ViT-B/16 | https://huggingface.co/openai/clip-vit-base-patch16 |
| | CLIP ViT-B/32 | https://huggingface.co/openai/clip-vit-base-patch32 |
| | CLIP ViT-L/14 | https://huggingface.co/openai/clip-vit-large-patch14 |
| | CLIP ViT-L/14-336px | https://huggingface.co/openai/clip-vit-large-patch14-336 |
| | OpenCLIP ViT-B/32 | https://huggingface.co/laion/CLIP-ViT-B-32-laion2B-s34B-b79K |
| | OpenCLIP ViT-H/14 | https://huggingface.co/laion/CLIP-ViT-H-14-laion2B-s32B-b79K |
| Text-to-image Model | OpenCLIP ViT-L/14 | https://huggingface.co/laion/CLIP-ViT-L-14-laion2B-s32B-b82K |
| | Stable Diffusion-v1.2 | https://huggingface.co/CompVis/stable-diffusion-v1-2 |
| | Stable Diffusion-v1.4 | https://huggingface.co/CompVis/stable-diffusion-v1-4 |
| | Stable Diffusion-base-v2.1 | https://huggingface.co/stabilityai/stable-diffusion-2-1-base |
| | Stable Diffusion-v2.1 | https://huggingface.co/stabilityai/stable-diffusion-2-1 |
| LLaVA [28, 29] | LLaVA-1.5-13B | https://huggingface.co/llava-hf/llava-1.5-13b-hf |